14 AFIT-CI-80-17T

AD A092364

REPORT DOCUMENTATION PAGE		READ INSTRUCTIONS BEFORE COMPLETING FORM
1. REPORT NUMBER 80-17T	2. GOVT ACCESSION NO. AD-A092 364	3. RECIPIENT'S CATALOG NUMBER
4. TITLE (and Subtitle) Slant Visual Range from Drop-size Distribution		5. TYPE OF REPORT & PERIOD COVERED THESIS/DISSERTATION
		6. PERFORMING ORG. REPORT NUMBER
7. AUTHOR(s) Edwin Stanley Arrance, Capt USAF		8. CONTRACT OR GRANT NUMBER(s) Master's thesis
9. PERFORMING ORGANIZATION NAME AND ADDRESS AFIT STUDENT AT: Texas A&M University		10. PROGRAM ELEMENT, PROJECT, TASK AREA & WORK UNIT NUMBERS 12 92
11. CONTROLLING OFFICE NAME AND ADDRESS AFIT/NR WPAFB OH 45433		12. REPORT DATE August 1980
		13. NUMBER OF PAGES 78
14. MONITORING AGENCY NAME & ADDRESS(if different from Controlling Office)		15. SECURITY CLASS. (of this report) UNCLASS
		15a. DECLASSIFICATION/DOWNGRADING SCHEDULE

LEVEL

16. DISTRIBUTION STATEMENT (of this Report)

APPROVED FOR PUBLIC RELEASE; DISTRIBUTION UNLIMITED

DTIC
ELECTE
DEC 3 1980

17. DISTRIBUTION STATEMENT (of the abstract entered in Block 20, if different from Report)

18. SUPPLEMENTARY NOTES

19. KEY WORDS (Continue on reverse side if necessary and identify by block number)

20. ABSTRACT (Continue on reverse side if necessary and identify by block number)

ATTACHED

012200   8011 24 061

DD FORM 1473   EDITION OF 1 NOV 65 IS OBSOLETE   UNCLASS

ABSTRACT

## Slant Visual Range From Drop-size Distribution

(1980, 78 pp)

Edwin Stanley Arrance, Captain, USAF

Master of Science, Texas A&M University

This research investigated the feasibility of obtaining visual range and slant visual range by use of drop-size distribution. The results of Davies' equation for computing visibility from drop-size distribution were compared to known values and those obtained from Mie scattering theory based on a program developed by Kattawar and Plass. Next, Davies' equation was applied to a Marshall-Palmer drop-size distribution and a vertically varying distribution obtained from a program developed by Borchers. The Marshall-Palmer distribution and visibility agree with those from Borchers' work. Davies' method of obtaining visibility then was used successfully to compute slant visual range along a glideslope. The drop-size distribution at various levels along the glideslope was produced by Borchers' program.

TEXAS A&M UNIVERSITY
DEPARTMENT OF
METEOROLOGY

SLANT VISUAL RANGE FROM DROP-SIZE DISTRIBUTION

A THESIS BY

EDWIN STANLEY ARRANCE

August 1980

SLANT VISUAL RANGE FROM

DROP-SIZE DISTRIBUTION

A Thesis

by

EDWIN STANLEY ARRANCE

Submitted to the Graduate College of
Texas A&M University
in partial fulfillment of the requirement for the degree of

MASTER OF SCIENCE

August 1980

Major Subject: Meteorology

80-171

The purpose of this questionnaire is to ascertain the value and/or contribution of research accomplished by students or faculty of the Air Force Institute of Technology (ATC). It would be greatly appreciated if you would complete the following questionnaire and return it to:

AFIT/NR
Wright-Patterson AFB OH 45433

Research Title: __Slant Visual Range from Drop-size Distribution__

Author: __Capt Edwin Stanley Arrance__

Research Assessment Questions:

1. Did this research contribute to a current Air Force project?

   a.   Yes   b.   No

2. Do you believe this research topic is significant enough that it would have been researched (or contracted) by your organization or another agency if AFIT had not?

   a.   Yes   b.   No

3. The benefits of AFIT research can often be expressed by the equivalent value that your agency achieved/received by virtue of AFIT performing the research. Can you estimate what this research would have cost if it had been accomplished under contract or if it had been done in-house in terms of manpower and/or dollars?

   a.   Man-years _____.   b. $_____

4. Often it is not possible to attach equivalent dollar values to research, although the results of the research may, in fact, be important. Whether or not you were able to establish an equivalent value for this research (3 above), what is your estimate of its significance?

   2. Highly   b. Significant   c. Slightly   d. Of No
      Significant   Significant   Significance

5. AFIT welcomes any further comments you may have on the above questions, or any additional details concerning the current application, future potential, or other value of this research. Please use the back of this questionnaire for your statement(s).

NAME   GRADE   POSITION

ORGANIZATION   LOCATION

USAF SCN 75-20B

SLANT VISUAL RANGE FROM

DROP-SIZE DISTRIBUTION

A Thesis

by

EDWIN STANLEY ARRANCE

Approved as to style and content by:

Dr. Vance E. Moyer
(Chairman of Committee)

Dr. George L. Huebner, Jr.   Dr. Glen N. Williams
(Member)   (Member)
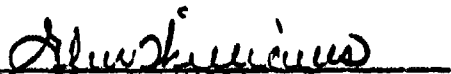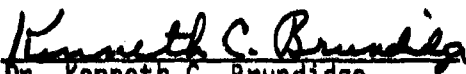
Dr. Kenneth C. Brundidge
(Head of Department)

August 1980

ABSTRACT

Slant Visual Range From Drop-size Distribution.   (August 1980)

Edwin Stanley Arrance, B.S., State University of New York

at Stony Brook, New York

Chairman of Advisory Committee: Dr. Vance E. Moyer

This research investigated the feasibility of obtaining visual range and slant visual range by use of drop-size distribution. The results of Davies' equation for computing visibility from drop-size distribution were compared to known values and those obtained from Mie scattering theory based on a program developed by Kattawar and Plass. Next, Davies' equation was applied to a Marshall-Palmer drop-size distribution and a vertically varying distribution obtained from a program developed by Borchers. The Marshall-Palmer distribution and visibility agree with those from Borchers' work. Davies' method of obtaining visibility then was used successfully to compute slant visual range along a glideslope. The drop-size distribution at various levels along the glideslope was produced by Borchers' program.

ACKNOWLEDGMENTS

DEDICATION

To the memory of my Mom and Dad, Julia and Harold Arrance.

TABLE OF CONTENTS

LIST OF TABLES

LIST OF FIGURES

1. INTRODUCTION

a. General

Many problems have been confronted by airplane pilots and some have been solved, but meteorological elements remain a limiting factor. Modern radars allow navigation around rainshowers, thunderstorms, hurricanes, and some other types of severe weather. Despite the introduction of automatic controls and landing aides, one element, visibility, continues to challenge the aircrew. If he cannot see the stripe down the middle of the runway to take off, or the runway itself when landing, the pilot waits for better conditions. When airborne, he may seek another location to land.

Visibility can be affected by different types of aerosols, moisture content, fog, and precipitation. Each can significantly alter visibility below the active minimum of an airfield. Pollution from a nearby plant, heavy rain from a storm, and dense fog can all close an airfield. Fog, however, can be the most devious and unpredictable over a long period of time. No guaranteed method of forecasting the horizontal visibility in fog has been found, and this becomes more difficult along the glideslope path of a landing aircraft.

The citations on this and the following pages follow the style of the <u>Journal of the Atmospheric Sciences</u>.

b. Background

Visibility measurements normally are made at the surface parallel to the active runway at an airfield. The most common procedure is to use a transmissometer with a 500-ft baseline to obtain values of runway visual range (RVR) when the horizontal surface visibility is less than or equal to 1.5 mi. This information then is made available to aircraft arriving at and departing from the airfield. As Lifsitz (1974(a)) pointed out, this will provide information about horizontal surface visibility beneath the glideslope of an aircraft. Problems develop because the transmissometer may or may not be placed in the approach zone and usually is not configured to measure along a slant path.

Early work by Koschmieder (as given in List, 1966) resulted in a theory for determining the visual range in the horizontal based on the extinction coefficient. Middleton (1952) summarized work in the area of visibility in the atmosphere. He covered the relation of visual range to liquid water content and showed that the drop-size distribution making up the liquid water content is critical to horizontal visibility. He then examined visibility from the pilot's point of view along a slant range. Early investigators used a search-light to investigate horizontal visual range and slant visual range (SVR).

Twomey and Howell (1965) studied the idea of monochromatic light versus white light for the measurement of visibility. A

transmissometer system aimed along the glideslope was used. Their
conclusions indicated that a monochromatic light source (laser) was
inferior to a heterochromatic (white) light source. Mie scattering
theory was used. Fenn (1966) attempted to relate atmospheric
extinction to atmospheric backscattering, but found no general rela-
tion. He did state, "The increase of visual range with a shift to
larger particles for constant total mass is well known from the rela-
tion holding for fog or cloud droplets, according to which the visual
range is proportional to the total liquid water content of the
cloud." Later Winstanley and Adams (1975) worked with a Point
Visibility Meter (PVM) to relate scattered light to extinction and
then visibility. Also in 1975, Davies related particle size and
mass distribution to visual range mathematically. He stated that
improper sampling of the particles could significantly affect the
results.

Plass and Kattawar (1968) used a Monte Carlo method with a
specific drop-size distribution and a given wavelength of incident
light to determine light scattering from cumulus clouds. In a later
article, Kattawar and Plass (1968) used six cloud models with
different particle-size distributions to demonstrate the effect
on transmitted and reflected light. Vogt (1968) also discussed the
use of backscattered light to measure visibility. He concluded
that an instrument measurement of backscattering could be used to
obtain visibility. Bertolotti et al. (1969) investigated the

use of a ruby laser to measure optical visibility. Their conclusion was that the laser would perform satisfactorily as long as fog was not present.

Ferrara et al. (1970) used a laser to measure the changes that occur in a fog drop-size distribution. They concluded that the main features of a fog distribution could be determined quickly in this way. Plass and Kattawar (1971) investigated the reflection of light from three different cloud models of appropriate particle-size distribution and concluded that the returned flux depends on the size distribution of the particles in the cloud. Dickson et al. (1975(a)) used a laser fog nephelometer to estimate drop-size distribution from measurements of the backscatter from the array of drops in real fog occurrences. This enabled them to calculate the horizontal visibility in kilometers from an average of

$$V = 3.912/\sigma \tag{1}$$

and

$$V = 2.996/\sigma, \tag{2}$$

as given in List (1966). In these equations, σ [km^{-1}] is the total extinction coefficient, rather than the scattering coefficient; it is determined from the drop-size distribution.

Viezee et al. (1972) made lidar observations at a slant range approximating the cockpit cutoff angle. They concluded that this approach provided operational measurements of slant range visibility. In a later report (1973) the same authors "... demonstrated that the

lidar could obtain detailed information on cloud conditions at remote locations along the approach path, where because of the marshes and open water, conventional ceilometers could not be operated." They also determined that reasonable values of visibility could be obtained. Lifsitz (1974(a)) investigated the use of a gallium-aluminum-arsenide (GaAlAs) lidar and a ruby lidar. He reported reasonable extinction coefficient values for the GaAlAs; however, the results were more limited in the case of the ruby lidar. He stated that, although extinction coefficients and therefore visibility could be determined with these lidar systems, the degree of confidence was not high. Moroz (1977) stated that "Lidar was shown conclusively to have excellent potential as a practical instrument for measurement of slant visual range ..." if it (1) could be made eye safe, (2) could have the effect of multiple scattering reduced during large attenuation situations, (3) could have a capability to reach the decision height, and (4) could be able to distinguish patchy fog and fog tops from continuous fog.

Another method under study is the use of forward scatter visibility meters (FSM) to obtain slant range visibility. In this case certain vertical levels are sampled. Lewis and Schlatter (1977) investigated the relationship of slant and runway visual range (RVR) by use of extinction-type transmissometers mounted at various heights on two towers along with wind and temperature sensors. They concluded that knowledge of the vertical density profile of fog would be useful

in estimating slant visual range. Lewis (1978), in a follow-on report based on the data from the original study, obtained horizontal transmittances at discrete vertical levels to compare to the 15-ft horizontal transmittance (more representative of current surface RVR measurements) instead of to the 5-ft horizontal transmittance. He concluded that "Measurements of atmospheric transmittance near the surface and at a level near 100, 125, or 150 ft can provide a basis for making operationally useful estimates of the SVR/RVR ratio." A recommendation to perform further studies relating to SVR/RVR ratios and the fog profile was included.

Work done by Burke (1979) also confirmed problems with use of a slanted transmissometer. "Unfortunately, the slanted position of the transmissometers often resulted in extinction coefficient values which were nonrepresentative of actual conditions during periods of precipitation." Problems developed with accumulation of liquid water within the tubes. Mooradian et al. (1979) discussed the propagation through fog by multiple scattering of a laser. Their primary interest was in optical communication.

Numerous researchers have investigated ways to obtain slant visual range with the goal of providing a better estimate of visibility to assist in aircraft control. The purpose of the present research is to attempt to bring together some of the ideas put forward and used by other researchers to compute visual range in a method which allows for comparison of results. This research will

analyze fog and damp haze conditions and a rainfall case. Primary emphasis will be from the point of view of a known drop-size distribution, which is converted to a visibility measurement. Most of the current research has used the lidar measurement method as opposed to the drop-size distribution method.

c. Procedure

Data on drop-size distribution and visibility obtained at the Capistrano Test Site in California (1974) [Dickson et al., 1975(a)] will be used to evaluate fog and damp haze situations. The drop-size distributions obtained by a fog nephelometer will be assumed homogeneous in the horizontal and vertical. Extinction will be calculated from Mie scattering theory in a program developed by Kattawar and Plass (1968) and then converted to a visibility. The value obtained by the program will be compared to the visibility values given in the Capistrano Test Site report. This will be used to verify the approach of computing visibility by drop-size distribution.

Next, a method reported by Davies (1975) for computing visual range will be used to calculate the visibility in the Capistrano case. Drop-size distribution will be the prime ingredient although his equations are indirectly based on the mass involved. These results will be compared to the Capistrano values and the Kattawar and Plass values.

Finally, a program developed by Borchers (1979) will be used to obtain a rainfall distribution of drop size with height. The

distribution will be considered homogeneous in the horizontal, but will vary in the vertical. Visibility will be computed by the Davies method in several layers and then applied to slant range to approximate the pilot's view. A Marshall-Palmer distribution also will be shown with calculated visibility for comparison with Borchers' surface results.

2. CAPISTRANO TEST CASE

a. Background

A laser fog nephelometer was used to measure drop-size distribution during April and May 1974 (Dickson et al., 1975(a)). The wavelength, 0.6328 μm, was produced by a helium neon (HeNe) laser beam. From the backscatter measurements obtained, a calculation of liquid water content and visibility was made. The air volume sampled was 1500 cm^3. The number of drops per nominal radius are shown in Table 1 on page 10 for two cases. One sample was at 0120 hours on 18 April 1974 during a case of relatively clear air. All times are given in local. The reported visibilities were approximately 0.5 km and 5.0 km, respectively. The visibility for each night is shown with time in Figure 1 on page 14. Figure 2 on page 15 shows the time variation of the number of droplets per cm^3.

A rapid variation in visibility around the times concerned can be seen in Table 2 on page 16. This gives visibility 10 min prior to, 10 min later than, and at 0120 hours as reported in the complete data set. This set shows a slightly greater number of drops at 0120 hours on 17 April with a correspondingly lower visibility. There appears to be a small discrepancy between the number of drops present at 0120 hours on 17 April as given in the complete Capistrano Test Site data set and as given separately by Dickson et al., (1975(a)) and Folster et al. (1975). Since the data were collected over a 5-min interval followed by a 5-min pause, some

Table 1. Channel Number and Nominal Radius (μm). [From Dickson et al., 1975(a)]

Channel Number	Nominal Radius	No. Drops[a] (1)*	No. Drops[a] (2)**
1	2.6	7	0
2	2.8	1290	3664
3	3.0	2929	4201
4	3.2	4095	2383
5	3.4	4383	1422
6	3.7	3993	918
7	4.0	3596	662
8	4.3	3262	513
9	4.6	3028	403
10	4.9	2897	378
11	5.3	2129	195
12	5.7	984	82
13	6.1	449	46
14	6.6	195	11
15	7.1	95	12
16	7.6	50	15
17	8.1	47	10
18	8.8	44	14
19	9.4	66	9
20	10.1	39	4

Table 1. Continued.

Channel Number	Nominal Radius	No. Drops[a] (1)*	No. Drops[a] (2)**
21	10.9	42	6
22	11.7	69	7
23	12.6	81	5
24	13.5	75	7
25	14.5	63	4
26	15.6	75	3
27	16.8	68	3
28	18.0	36	4
29	19.4	59	2
30	20.8	45	0
31	22.4	46	0
32	24.0	46	2
33	25.8	52	2
34	27.8	48	0
35	29.8	24	0
36	32.1	29	0
37	34.5	26	0
38	37.1	26	0
39	39.8	36	0
40	42.8	30	0
41	46.0	31	0

Table 1. Continued.

Channel Number	Nominal Radius	No. Drops[a] (1)*	No. Drops[a] (2)**
42	49.4	23	0
43	53.1	26	0
44	57.1	22	0
45	61.4	24	0
46	66.0	9	0
47	70.9	7	0
48	76.2	12	0
49	81.9	9	0
50	88.1	2	0
51	94.6	1	0
52	102.0	1	0
53	109.0	3	0
54	118.0	1	0
55	126.0	0	0
56	136.0	0	0
57	146.0	0	0
58	157.0	0	0
59	169.0	0	0
60	181.0	0	0
61	195.0	0	0

Table 1. Continued.

Channel Number	Nominal Radius	No. Drops[a] (1)*	No. Drops[a] (2)**
62	210.0	0	0
63	225.0	0	0
64	242.0	0	0

* (1) 0120 hours 17 April Fog Data.

** (2) 0120 hours 18 April Relatively Clear Air Data.

[a] Number of drops per 1500 cm^3.
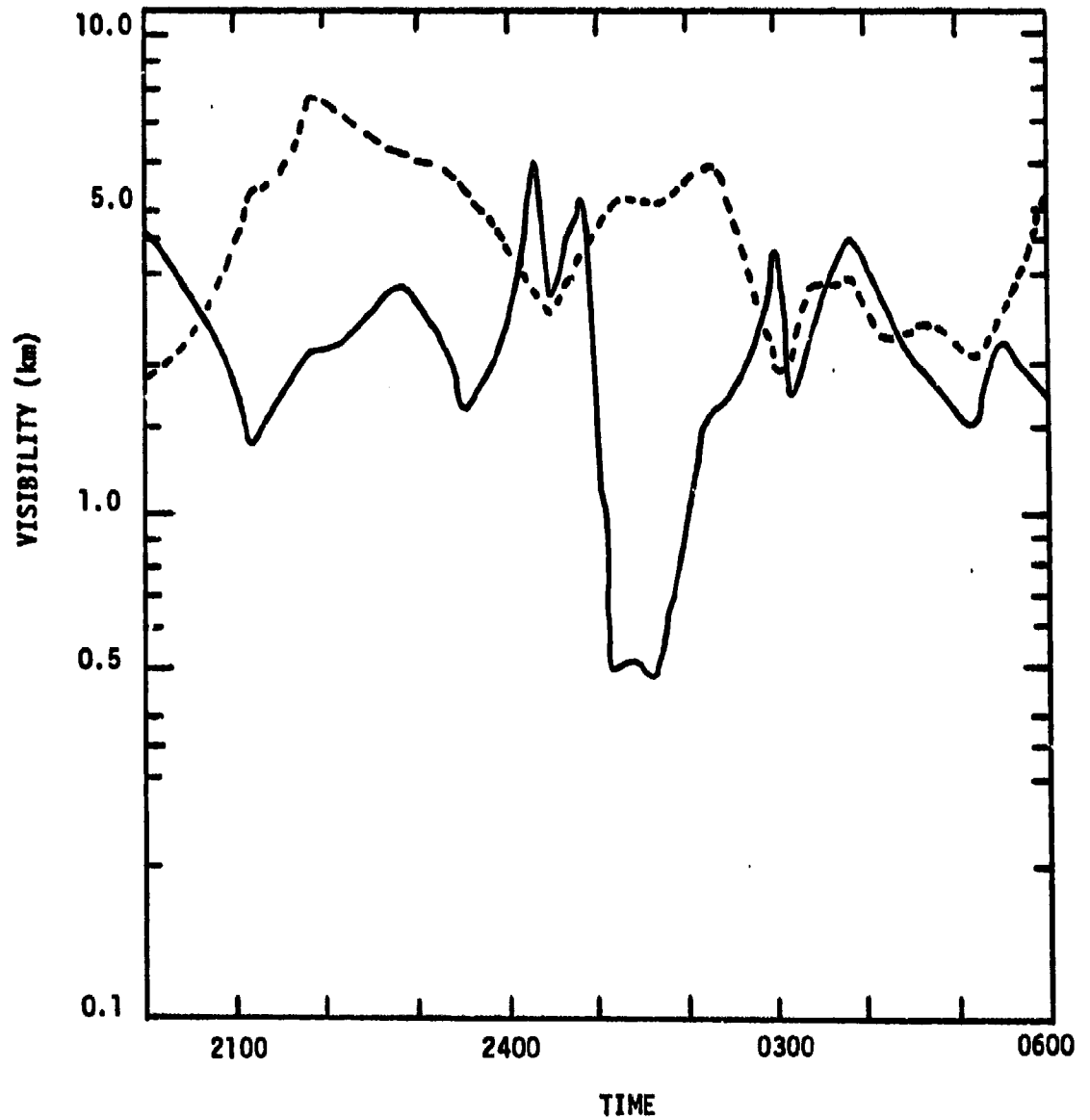
Fig. 1. Visibility variation with local time. [From Dickson
et al., 1975(a)]

—— Fog Data
--- Relatively Clear Air Data
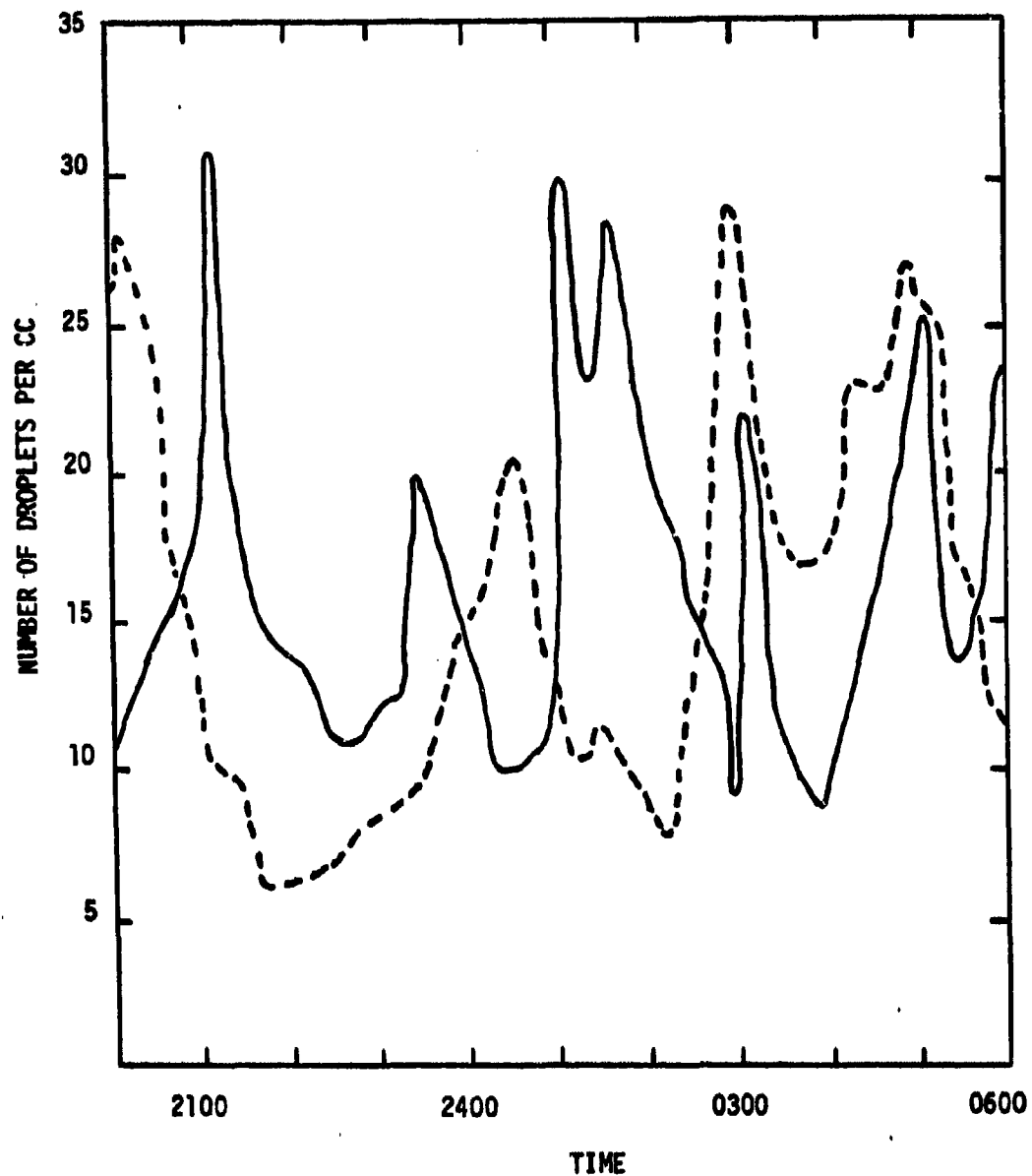
Fig. 2.   Total number of water droplets as a function of local time.
[From Dickson et al., 1975(a)]

————Fog Data
-----Relatively Clear Air Data

of the data may have been marked with the incorrect time or may have been misprinted. The value of 0.378 km (Table 2, p. 16) was given in the complete data set. The reference in the footnote (Table 2) to a value of 0.5 km is based on the value taken off Fig. 1 (p. 14). This figure appeared in both the Dickson et al. and Folster et al. works. It may be that the difference results from smoothing, so that erratic fluctuations do not appear over short time periods.

Table 2. Reported visibility variation with time for Capistrano Test Site.

Time	17 April	18 April
0110	0.518 km	4.217 km
0120	0.378 km*	4.516 km
0130	0.573 km	3.820 km

Values are averages of the results obtained from the List (1966) equations.
* Value based on Fig. 1 (p. 14) gives about 0.5 km.

b. Kattawar and Plass Method

Kattawar and Plass (1968) used their computer program to analyze reflected light and light scattering in various drop-size distributions and cloud models. Incident light of a given wavelength was followed by using a Monte Carlo method and complex Mie scattering theory. Input to the program included the drop-size distribution to

be analyzed, the index of refraction (1.3318-0.01), wavelength
(0.6328 μm), size parameter minimum and maximum values of the
range being investigated, number of evaluation points in this range,
and the number of points evaluated between the maximum and a slightly
higher value to check on the convergence of the values compared to
the input data. Details of the program will not be discussed. Output
of the program included values of average total cross section, average
scattering cross section, average radius, absorption (assumed to be
zero in this research), single scattering albedo, polarization, and
a scattering function (scalar phase function). The relationship
used to calculate an extinction coefficient $[km^{-1}]$, σ, is given by

$$\sigma = (\lambda/2\pi)^3 \ (1/1500) \int n(x)\pi x^2 \ Q_{EXT}(x)dx \ . \qquad (3)$$

In (3) the integrand represents the average total cross section.
The factor (1/1500) is to reduce n(x), the number of particles per
size parameter interval, to units of per cubic centimeter. The size
parameter is defined as $x = 2\pi r/\lambda$ where r is the radius of a particle
in microns and λ is the wavelength in microns. $Q_{EXT}(x)$ is the
extinction efficiency of the given size parameter. The visual
range, V, in kilometers is then obtained from

$$V = 1/\sigma. \qquad (4)$$

As can be seen in Table 3, the value for the relatively clear
air case of 18 April is closer to the Capistrano reported value of
4.516 km than to the fog case value of 0.5 km. The total spectrum
of drops was not used in this method in order to reduce computer
costs. A complete computer run with total convergence of the data

curve should yield improved results, but would be very expensive to run over the total distribution. The percentage of the distribution used in each run is shown in Table 3.

Table 3. Computed visibility and percent of total drops used in Kattawar and Plass method.

Time	0120 hours	0120 hours
Date	17 April	18 April
Visual Range	0.421 km	4.452 km
% of total drops used in calculation	99.02%	99.97 %

Considering that the value of 0.5 km was taken from Fig. 1 and is an average, the low visibility value obtained from the program appears reasonable since the result is not smoothed. Thus the program results for the high and low visibility cases compare favorably with the Capistrano values. The Kattawar and Plass method requires the drop-size distribution to calculate theoretically first the back-scattering, then the extinction, and finally the visibility. The Capistrano drop-size distribution was obtained by physically measuring the backscatter, inferring the distribution, and then calculating the visibility. The first method requires knowledge of the drop-size distribution beforehand, while the second starts by inferring the distribution from a measurement or observation. In

effect, the methods are similar. This permits the use of theory to verify the experimental values, or vice versa.

Graphs of the scattering function versus scattering angle in degrees for both cases are given in Fig. 3 and Fig. 4. It can be seen that for the fog case the scattering function exceeds that for the clear air case by an order of magnitude. Mooradian et al. (1979) state that "Calculations using Mie theory show that the scalar phase function for real maritime fog distributions are highly peaked in the forward direction, thereby suggesting a strong forward-scatter component of the scattered radiation in the vicinity of the line-of-sight axis." These figures also verify that the program is showing a relatively clear air case and then a maritime fog case. Inclusion of all 100% of the drops should peak the function even more.

c. Davies Method

Davies (1975) based his paper on the fact that the product of mass concentration of an aerosol and visual range are constant for a given drop-size distribution. If computations are made for individual size ranges, these are additive and inversely proportional to the visual range. In developing his equation, Davies used the Koschmieder relation of

$$V = 3.9/\bar{\sigma}, \tag{5}$$

where $\bar{\sigma}$ is the extinction coefficient per kilometer averaged over all particles and V is the visual range in kilometers. He also used the wavelength λ equal to 0.5500 μm for his calculations. This is

Scattering Angle in Degrees

0   20   40   60   80   100   120   140   160   180

10^4 10^3 10^2 10^1 10^0 10^{-1} 10^{-2} 10^{-3}

Scattering function
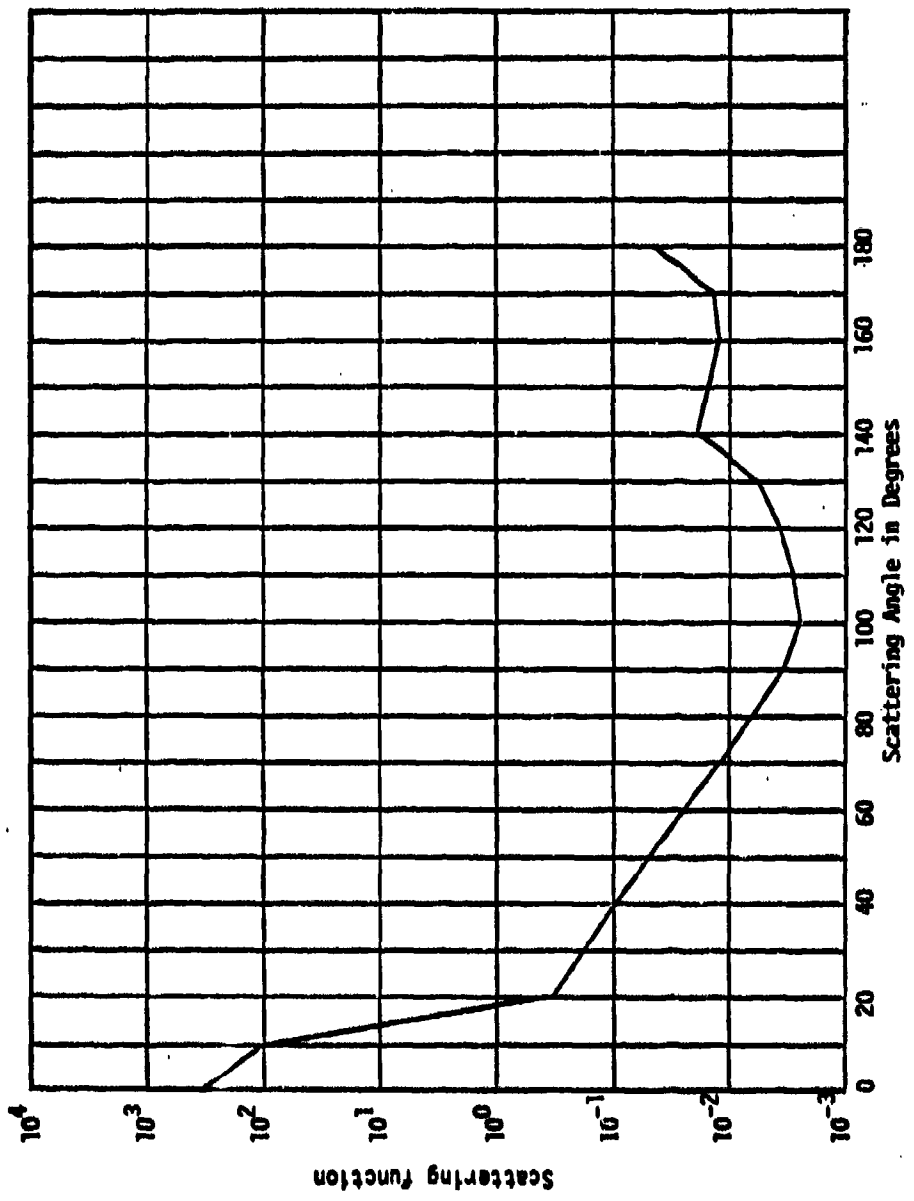
Fig. 3. Scattering function for clear air data.
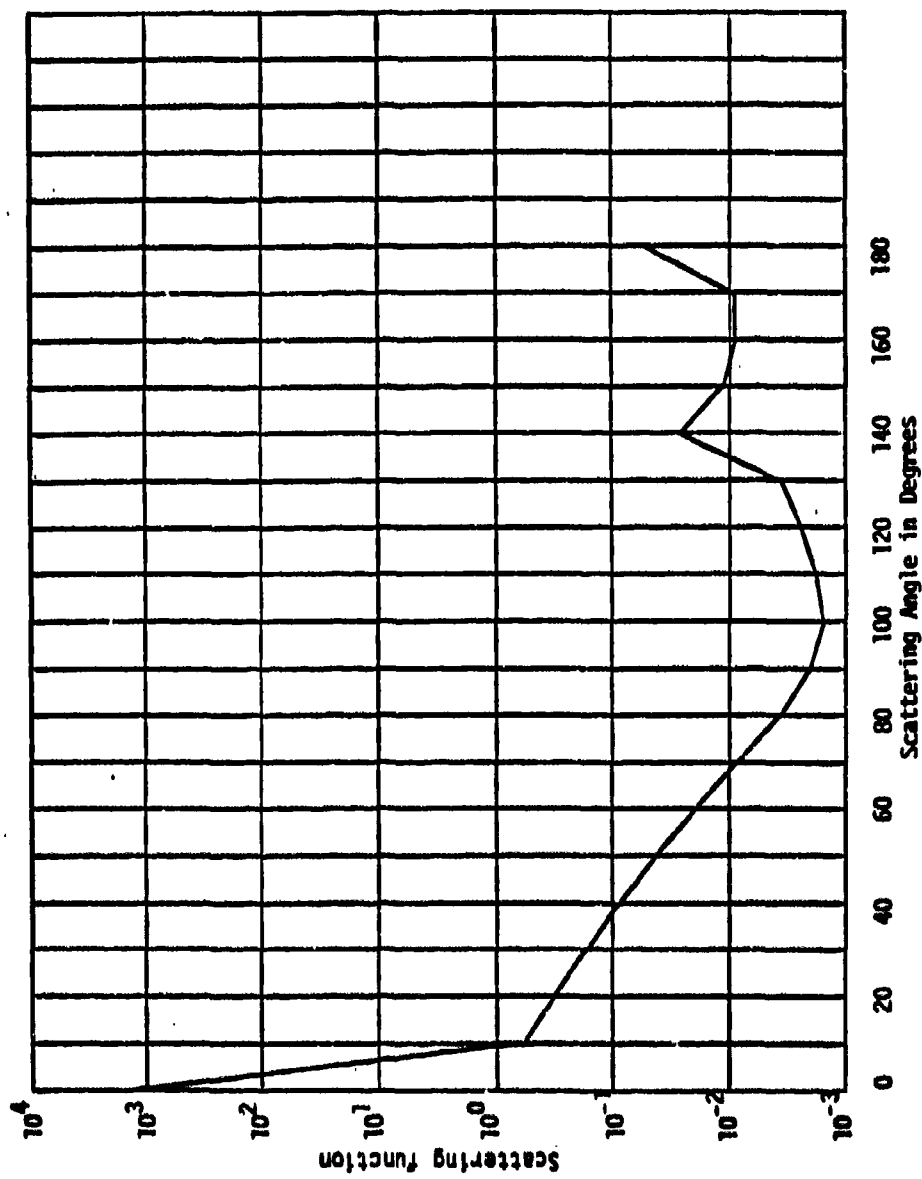
Fig. 4. Scattering function for fog.

in the peak of the visible spectrum, and only a slight variation in results would be expected on either side of this value.

Finally Davies arrived at the equation

$$\Sigma\,(1/V_i) = (\pi/3.9)\,(10^{-6})\,\Sigma\,n_i r_i^2 E_i, \tag{6}$$

where for the ith interval, n_i is the number of particles per cubic centimeter, r_i is the radius in microns, E_i is the extinction efficiency, and V_i is the visual range in meters. The extinction efficiency with a refractive index of 1.3318 and zero absorption is approximately equal to 2.0 for the size parameter range involved. This was used throughout the present calculations. Table 4 lists the values by term for each interval of the 18 April case of relatively clear air. The resultant visual range is 5.086 km, which compares very well with both the Capistrano report and the Kattawar and Plass program solution. Table 5 lists the values by term for each interval of the 17 April fog case. The visual range is 0.541 km, which compares better with the Capistrano report of 0.5 km than with the Kattawar and Plass program. Since Davies' equation is solved by using all drops and the total mass while the program used only 99% of the drops, some deviation is expected.

This chapter has shown that the three methods have all yielded comparable values of visual range. As noted previously, the Capistrano data were obtained by measuring the backscatter to obtain the drop-size distribution and then to calculate the visual range. The Kattawar and Plass method takes an assumed drop-size distribution

Table 4. Values used in Davies' equation at various radii to calculate the clear air case of Capistrano Test Site visibility. Data for 0120 hours on 18 April 1974.

Radius[a]	$n(r)$[b]	$\dfrac{n(r)r_i^2}{1500}$ [c]	E_i	$\dfrac{n(r)r_i^2 E_i}{1500}$ [c]	$\dfrac{1}{V_i}$ [d]
2.6	0	0.0	2.0	0.0	0.0
2.8	3664	1.9151×10^1	2.0	3.8301×10^1	3.0853×10^{-5}
3.0	4201	2.5206×10^1	2.0	5.0412×10^1	4.0609×10^{-5}
3.2	2383	1.6268×10^1	2.0	3.2536×10^1	2.6209×10^{-5}
3.4	1422	1.0959×10^1	2.0	2.1918×10^1	1.7656×10^{-5}
3.7	918	8.3787	2.0	1.6757×10^1	1.3498×10^{-5}
4.0	662	7.0613	2.0	1.4123×10^1	1.1376×10^{-5}
4.3	513	6.3236	2.0	1.2647×10^1	1.0188×10^{-5}
4.6	403	5.6850	2.0	1.1370×10^1	9.1589×10^{-6}
4.9	378	6.0505	2.0	1.2101×10^1	9.7479×10^{-6}
5.3	195	3.6517	2.0	7.3034	5.8832×10^{-6}
5.7	82	1.7761	2.0	3.5522	2.8615×10^{-6}
6.1	46	1.1411	2.0	2.2822	1.8384×10^{-6}
6.6	11	3.1944×10^{-1}	2.0	6.3888×10^{-1}	5.1464×10^{-7}
7.1	12	4.0328×10^{-1}	2.0	8.0656×10^{-1}	6.4971×10^{-7}
7.6	15	5.7760×10^{-1}	2.0	1.1552	9.3056×10^{-7}
8.1	10	4.3740×10^{-1}	2.0	8.7480×10^{-1}	7.0468×10^{-7}
8.8	14	7.2277×10^{-1}	2.0	1.4455	1.1644×10^{-6}
9.4	9	5.3016×10^{-1}	2.0	1.0603	8.5413×10^{-7}

Table 4. Continued.

Radius[a]	$n(r)$[b]	$\dfrac{n(r)r_i^2}{1500}$ [c]	E_i	$\dfrac{n(r)r_i^2 E_i}{1500}$ [c]	$\dfrac{1}{V_i}$ [d]
10.1	4	2.7203×10^{-1}	2.0	5.4405×10^{-1}	4.3825×10^{-7}
10.9	6	4.7524×10^{-1}	2.0	9.5048×10^{-1}	7.6565×10^{-7}
11.7	7	6.3882×10^{-1}	2.0	1.2776	1.0292×10^{-6}
12.6	5	5.2920×10^{-1}	2.0	1.0584	8.5258×10^{-7}
13.5	7	8.5050×10^{-1}	2.0	1.7010	1.3702×10^{-6}
14.5	4	5.6067×10^{-1}	2.0	1.1213	9.0328×10^{-7}
15.6	3	4.8672×10^{-1}	2.0	9.7344×10^{-1}	7.8414×10^{-7}
16.8	3	5.6448×10^{-1}	2.0	1.1290	9.0942×10^{-7}
18.0	4	8.6400×10^{-1}	2.0	1.7280	1.3920×10^{-6}
19.4	2	5.0181×10^{-1}	2.0	1.0036	8.0846×10^{-7}
20.8	0	0.0	2.0	0.0	0.0
22.4	0	0.0	2.0	0.0	0.0
24.0	2	7.6800×10^{-1}	2.0	1.5360	1.2373×10^{-6}
25.8	2	8.8752×10^{-1}	2.0	1.7750	1.4299×10^{-6}
27.8	0	0.0	2.0	0.0	0.0

$\Sigma n(r) = 14987$ $\qquad\qquad\qquad\qquad\qquad \Sigma \dfrac{1}{V_i} = 1.9662 \times 10^{-4}\ m^{-1}$

Note: The number 1500 is a factor to reduce the volume so $n(r)$ is in number of drops per cubic centimeter.
[a] Units in microns.
[b] Number of drops/1500 cm^3.
[c] Number of drops/cm.
[d] m^{-1}.

Table 5. Values used in Davies' equation at various radii to calculate the fog case of Capistrano Test Site visibility. Data for 0120 hours on 17 April 1974.

Radius[a]	$n(r)$[b]	$\dfrac{n(r)r_1^2}{1500}$[c]	E_1	$\dfrac{n(r)r_1^2 E_1}{1500}$[c]	$\dfrac{1}{V_1}$[d]
2.6	7	3.1547×10^{-2}	2.0	6.3093×10^{-2}	5.0824×10^{-8}
2.8	1290	6.7424	2.0	1.3485×10^{1}	1.0862×10^{-5}
3.0	2929	1.7574×10^{1}	2.0	3.5148×10^{1}	2.8313×10^{-5}
3.2	4095	2.7955×10^{1}	2.0	5.5910×10^{1}	4.5038×10^{-5}
3.4	4383	3.3778×10^{1}	2.0	6.7557×10^{1}	5.4419×10^{-5}
3.7	3993	3.6443×10^{1}	2.0	7.2886×10^{1}	5.8712×10^{-5}
4.0	3596	3.8357×10^{1}	2.0	7.6715×10^{1}	6.1796×10^{-5}
4.3	3262	4.0210×10^{1}	2.0	8.0419×10^{1}	6.4781×10^{-5}
4.6	3028	4.2715×10^{1}	2.0	8.5430×10^{1}	6.8817×10^{-5}
4.9	2897	4.6371×10^{1}	2.0	9.2743×10^{1}	7.4708×10^{-5}
5.3	2129	3.9869×10^{1}	2.0	7.9738×10^{1}	6.4232×10^{-5}
5.7	984	2.1313×10^{1}	2.0	4.2627×10^{1}	3.4338×10^{-5}
6.1	449	1.1506×10^{1}	2.0	2.3013×10^{1}	1.8538×10^{-5}
6.6	195	5.6628	2.0	1.1326×10^{1}	9.1232×10^{-6}
7.1	95	3.1926	2.0	6.3853	5.1436×10^{-6}
7.6	50	1.9253	2.0	3.8507	3.1019×10^{-6}
8.1	47	2.0558	2.0	4.1116	3.3120×10^{-6}
8.8	44	2.2716	2.0	4.5431	3.6597×10^{-6}
9.4	66	3.8878	2.0	7.7757	6.2636×10^{-6}
10.1	39	2.6523	2.0	5.3045	4.2730×10^{-6}

Table 5. Continued.

Radius[a]	$n(r)$[b]	$\dfrac{n(r)r_1^2}{1500}$[c]	E_1	$\dfrac{n(r)r_1^2 E_1}{1500}$[c]	$\dfrac{1}{V_1}$[d]
10.9	42	3.3267	2.0	6.6534	5.3595×10^{-6}
11.7	69	6.2969	2.0	1.2594×10^1	1.0145×10^{-5}
12.6	81	8.5730	2.0	1.7146×10^1	1.3812×10^{-5}
13.5	75	9.1125	2.0	1.8225×10^1	1.4681×10^{-5}
14.5	63	8.8305	2.0	1.7661×10^1	1.4227×10^{-5}
15.6	75	1.2168×10^1	2.0	2.4336×10^1	1.9604×10^{-5}
16.8	68	1.2795×10^1	2.0	2.5590×10^1	2.0613×10^{-5}
18.0	36	7.7760	2.0	1.5552×10^1	1.2528×10^{-5}
19.4	59	1.4803×10^1	2.0	2.9607×10^1	2.3850×10^{-5}
20.8	45	1.2979×10^1	2.0	2.5958×10^1	2.0910×10^{-5}
22.4	46	1.5387×10^1	2.0	3.0775×10^1	2.4790×10^{-5}
24.0	46	1.7664×10^1	2.0	3.5328×10^1	2.8458×10^{-5}
25.8	52	2.3076×10^1	2.0	4.6151×10^1	3.7176×10^{-5}
27.8	48	2.4731×10^1	2.0	4.9462×10^1	3.9843×10^{-5}
29.8	24	1.4209×10^1	2.0	2.8417×10^1	2.2891×10^{-5}
32.1	29	1.9921×10^1	2.0	3.9843×10^1	3.2095×10^{-5}
34.5	26	2.0631×10^1	2.0	4.1262×10^1	3.3238×10^{-5}
37.1	26	2.3858×10^1	2.0	4.7716×10^1	3.8437×10^{-5}
39.8	36	3.8017×10^1	2.0	7.6034×10^1	6.1248×10^{-5}
42.8	30	3.6637×10^1	2.0	7.3274×10^1	5.9025×10^{-5}
46.0	31	4.3731×10^1	2.0	8.7461×10^1	7.0453×10^{-5}

Table 5. Continued.

Radius[a]	n(r)[b]	$\frac{n(r)r_1^{2}[c]}{1500}$	E_1	$\frac{n(r)r_1^{2}E_1[c]}{1500}$	$\frac{1}{V_1}$[d]
49.4	23	3.7419×10^1	2.0	7.4838×10^1	6.0285×10^{-5}
53.1	26	4.8873×10^1	2.0	9.7746×10^1	7.8738×10^{-5}
57.1	22	4.7819×10^1	2.0	9.5639×10^1	7.7040×10^{-5}
61.4	24	6.0319×10^1	2.0	1.2064×10^2	9.7179×10^{-5}
66.0	9	2.6136×10^1	2.0	5.2272×10^1	4.2107×10^{-5}
70.9	7	2.2458×10^1	2.0	4.6917×10^1	3.7793×10^{-5}
76.2	12	4.6452×10^1	2.0	9.2903×10^1	7.4837×10^{-5}
81.9	9	4.0246×10^1	2.0	8.0491×10^1	6.4839×10^{-5}
88.1	2	1.0349×10^1	2.0	2.0698×10^1	1.6673×10^{-5}
94.6	1	5.9661	2.0	1.1932×10^1	9.6118×10^{-6}
102.0	1	6.9360	2.0	1.3872×10^1	1.1174×10^{-5}
109.0	3	2.3762×10^1	2.0	4.7524×10^1	3.8282×10^{-5}
118.0	1	9.2827	2.0	1.8565×10^1	1.4955×10^{-5}
126.0	0	0.0	2.0	0.0	0.0

$\Sigma n(r) = 34725$ $\Sigma \frac{1}{V_1} = 1.8464 \times 10^{-3}$ m^{-1}

Note: The number 1500 is a factor to reduce the volume so n(r) is in number of drops per cubic centimeter.

[a] Units in microns.
[b] Number of drops/1500 cm^3.
[c] Number of drops/cm.
[d] m^{-1}.

and uses scattering theory to calculate the extinction from which
the visibility is determined. Davies used a particle mass relation-
ship and the Koschmieder function combined with a drop-size distribu-
tion to compute the visual range. Although similar in some aspects,
they are variations of solving the problem of how to find the visual
range. Table 6 shows a comparison of the results for all three methods.

Table 6. Comparison of Capistrano, Kattawar and Plass, and Davies'
visibilities for the fog and clear air cases at Capistrano
Test Site.

Time	Date	Capistrano	Kattawar and Plass	Davies
0120 hours	17 April	0.500 km	0.421 km	0.541 km
0120 hours	18 April	4.516 km	4.452 km	5.086 km

Another reason for the variation in values from the Capistrano
method is the fact that the fog nephelometer has a lower-level
discrimination of approximately 3 μm. In other words, it does not
measure well below this level and probably does not show all the
drops that are present. As Davies (1975) states, "Failure to
include fine droplets and particles accounts for measured visual
ranges sometimes being lower than calculated values." Thus the
Davies values show higher visual range due to exclusion of the smaller
drops. At the same time, the Kattawar and Plass program is looking

at an interval which is not dependent on the small values. It gives almost the same to slightly smaller values than reported in the complete data set at Capistrano (Dickson et al., 1975(a)). This implies that this method is giving a visibility based on inclusion of the smaller drops even though they were not measured.

3. RAINFALL CASES

a. Borchers' Data

During the attempt to use Borchers' program, a major problem developed. The number of drops per radius interval, when used in the Davies method, gave a visibility that appeared to be too low. At a 25 mm/hr rainfall rate, the calculated visibility was 208.60 m. The table of calculation (Table A1) and the visibility calculations are shown in Appendix A.

A possible explanation for this problem may lie in the neglect of collisional breakup in the program. Another problem may be that this program assumes a downdraft. The effect of a downdraft has not been considered in this research. A downdraft may increase the moisture content of the subcloud air by physically transporting additional liquid water drops. This would cause more drops to be present than would be expected. On the other hand, a downdraft may lead to a drying and evaporation of some drops through compressional heating. The downward motion also may concentrate the rainfall in a rainshaft which would lead to a greater number of drops than expected. Borchers' "... program determines the change that occurs in a Marshall-Palmer raindrop-size distribution due to evaporation, collision-coalescence, aerodynamic breakup, ... as the drop falls in a constant subcloud downdraft... ." The rainfall rate was 25 mm/hr (about 1 in./hr) and the downdraft was 5 m/sec. The future inclusion of collisional breakup should improve the results. How much of an

effect the downdraft has on visibility is undetermined at this time.

Additional calculations were made at 100 m and 200 m above the surface. These are included in Table A2 and Table A3, along with their respective visibility calculations, in Appendix A. Table 7 summarizes the results. Some evaporation is taking place as the drop falls and this helps to account for fewer drops at the surface.

Table 7.   Summary of Borchers' program data for 25 mm/hr rainfall rate.

Level	# drops/m^3	Visibility (0.0424-4.3046 mm)	Visibility (0.8542-2.1524 mm)
Surface	1.0692×10^5	208.60 m	1241.77 m
100 m	1.1221×10^5	203.02 m	1222.5 m
200 m	1.1821×10^5	197.48 m	1203.8 m

b. Marshall-Palmer Data

To see if the Davies equation can be used on a rainfall distribution, it was decided to test it against the Marshall-Palmer distribution. The equation used appears in McCartney (1976) and is

$$N(D) = N_0 \exp(-\Lambda D), \tag{7}$$

where

$$N_0 = 8 \times 10^3 \text{ m}^{-3} \text{ mm}^{-1},$$
$$\Lambda = 4.1R^{-0.21} \text{ mm}^{-1}.$$

R is the rainfall rate in mm/hr, D is the diameter of the drop, N_0 is the intersection point when the diameter is zero, and N(D) is the number of drops in the given diameter interval. Calculations were made for values of R equal to 5, 12, 25, 50 and 100 mm/hr. Tables B1 thru B5 show the results per radius interval. These are given in Appendix B along with the calculation of visibilities for each rate.

The radius intervals investigated are based on the following statement from McCartney (1976): "Cole et al. (1969) state that this function has the greatest validity for drops having diameters between 0.75 and 2.25 mm for rainfall rates of about 1 mm/hr, between 1.25 and 3 mm for rates near 5 mm/hr, and between 1.5 and 4.5 mm for rates greater than 25 mm/hr." Since the function is exponential it will overestimate the number of small and large drops. To allow a meaningful comparison between rainfall rates, the visibility was computed within the above intervals.

A 0.100-mm interval is used to simulate the measurable interval of drop radii. The choice of interval will make a significant difference in the visibility obtained by the Davies equation. The results found are listed in Table 8 on page 33. The last column on the right shows the increase in visibility that would occur when the radius interval is doubled from 0.100 mm to 0.200 mm. The visibility values appear realistic for the given rainfall rates.

Table 8.   Summary of Marshall-Palmer visibilities.

Rainfall Rate	Radius Range Investigated	Visibility (0.100 radius)	Visibility (0.200 radius)
5 mm/hr	0.625-1.525 mm	2278.1 m	3912.3 m
12 mm/hr	0.750-2.250 mm	1327.6 m	2332.4 m
25 mm/hr	0.750-2.250 mm	644.1 m	1162.1 m
50 mm/hr	0.750-2.250 mm	345.6 m	637.0 m
100 mm/hr	0.750-2.250 mm	195.5 m	367.1 m

Table 9.   Summary of Marshall-Palmer visibility versus number of drops.

Rainfall Rate	Number of Drops	Visibility
5 mm/hr	4.6580×10^2	2278.1 m
12 mm/hr	5.3660×10^2	1327.6 m
25 mm/hr	1.0259×10^3	644.1 m
50 mm/hr	1.7624×10^3	345.6 m
100 mm/hr	2.8628×10^3	195.5 m

An advantage of the Davies equation is that a given drop-size distribution may be converted readily to a visibility. A disadvantage of using the Marshall-Palmer equation occurs with selecting the radius intervals. The latter equation will provide a spectrum of drops from zero to infinity; however, not all these values would be measured. There also will be a natural cutoff in droplet sizes due to oscillatory breakup as the drops fall.

One major problem may exist with using the Davies equation. In his development, Davies states that particle sizes cover a range of 10^5 µm; however, the equations are tested against a mist or fog. A formal restriction is not placed on the size radius that may be used in his equations. Since Davies states in his introduction that "... there has, however, been little discussion of the influence of particle size upon visual range, at given mass concentration of aerosol, a feature which may help to characterize the particles." This research has tried to show the results obtained when applying Davies' work to various rainfall rates. It seems logical that a successful extension could be made. Modification to Davies' equation, similar to those done by other researchers using the Marshall-Palmer equation, should produce viable results under differing conditions. A controlled experiment would be needed to test this postulate.

Experience has shown that initially poor visibility may improve at the onset of rainfall. This may be explained as a scavenging from the atmosphere through various mechanisms of other particles

(aerosols, pollution, hydrosols) by the raindrops. The calculated cases included only the instantaneous raindrop distribution, so the change in total particles is not included in the results. When the rainfall rate is increased, there is an increase in the number of drops with a corresponding drop in visibility. Table 9 on page 33 relates rainfall rate to visibility. It can be stated, therefore, that if other aerosols or hydrosols are present when a steady rain starts, there will be an increase in the visibility until the "pure rain" state is reached. Another complicating factor would be the presence of fog or drop splatter (spray) on surfaces that would affect the visibility. As an observer looks at a visibility marker, the contributions of each would be inseparable.

c. Comparison of Borchers' and Marshall-Palmer Results

Two visibility columns appear in Table 7 (p. 31). The first includes all 41 radius values with reported drop concentrations. The second looks only at the results from 0.8542 mm to 2.1524 mm. This parallels the range used for the Marshall-Palmer calculations in Table B3 (p. 67). Taking the Marshall-Palmer values at intervals of 0.200 mm to approximate more closely the program intervals gives a Borchers visibility of 1241.77 m at the surface and a Marshall-Palmer visibility of 1162.1 m. These results are quite comparable. Thus the Borchers program appears to give distributions and visibilities similar to Marshall-Palmer.

Borchers' results in the vertical also will be considered representative of real-world conditions in order to show that drop-size distributions can be used to infer slant range visibility.

4. SLANT RANGE VISIBILITY

a. General

Slant range visibility is the visibility along the glideslope of an aircraft arriving at or departing from an airfield. This visibility value does not have to coincide with the horizontal surface visibility or vertical visibility reported in the local observation. The glideslope is depicted geometrically in Figure 5 on page 38. Table 10 on page 39 shows the variation in distance between horizontal and glideslope compared to the approach points of the aircraft (points E, C, F on Fig. 6) for various approach angles. Note the large difference between the height above ground and the distance along the glideslope. This explains why a pilot may report that the runway is visible as he flies over the field and then reports it not visible when making the final approach down the glideslope. Even a vertically shallow layer of obstruction to visibility can cause problems. Surface visibility may even be better than the slant visual range along the glideslope.

b. Borchers' Data Applied to Glideslope.

Figure 6 on page 40 shows the schematic with Borchers' data entered for three levels. The number of drops and visibility are considered to be uniform in the horizontal and for 100-m vertical sections. This means the values calculated at 200 m are applied to the 100-m layer from 200 m above the surface to the 300-m level.
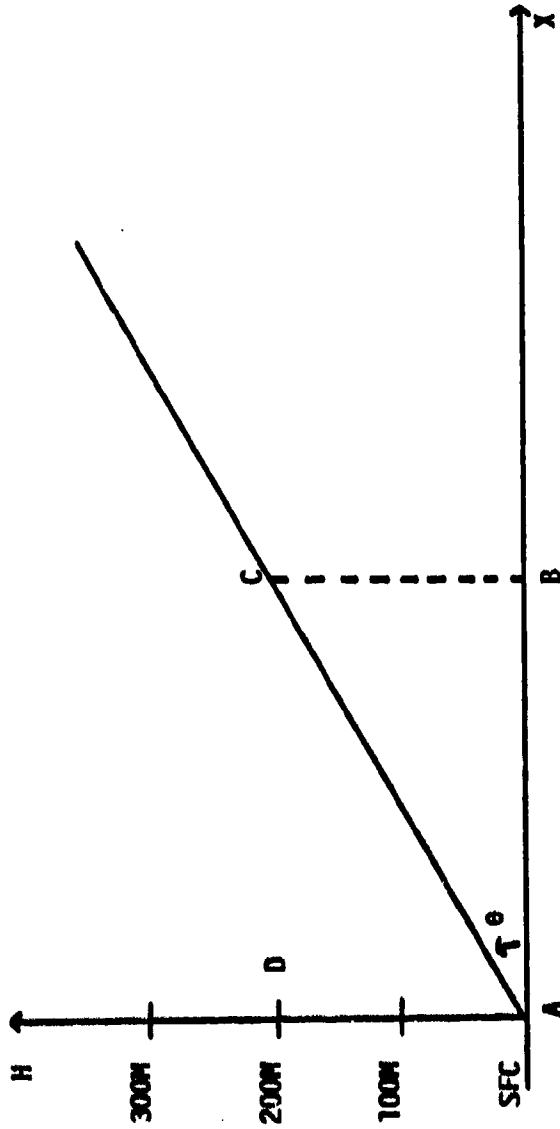
Fig. 5. Glideslope for siant range visibility.

θ = Glideslope angle
X = Horizontal direction
H = Vertical height
AC = Glideslope for slant visual range (SVR)
C = Altitude of beginning encounter
AD = Vertical visibility
AB = Surface visibility (RVR)

Table 10. Horizontal versus glideslope distances with varying
glideslope angle, θ, from Fig. 6.

θ	Height	Horizontal Distance	Slant Distance
Angle (deg)	EH (m)	AH (m)	AE (m)
3	300	5724.34	5732.20
12	300	1411.39	1442.92
15	300	1119.62	1159.11
Angle (deg)	CB (m)	AB (m)	AC (m)
3	200	3816.23	3821.46
12	200	940.93	961.95
15	200	746.41	772.74
Angle (deg)	FG (m)	AG (m)	AF (m)
3	100	1908.11	1910.73
12	100	470.46	480.97
15	100	373.21	386.37
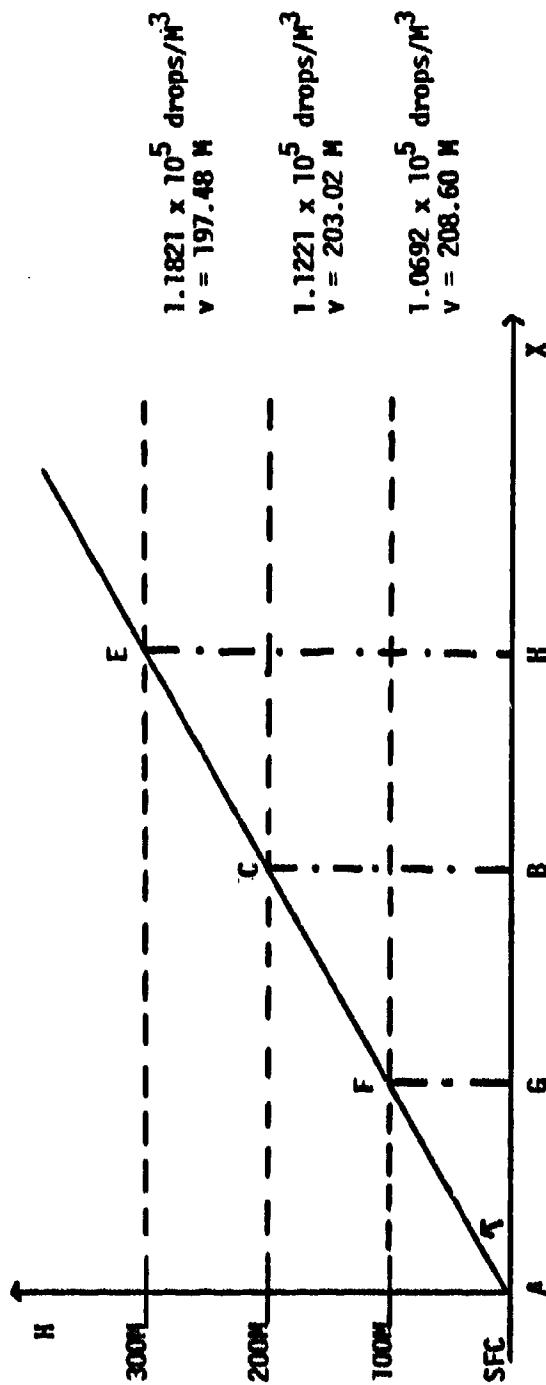
Fig. 6. Slant visual range with Borchers' program data shown.

Looking along the slant path will give visibilities which are lower than at the surface. This can be verified by summing the effect of the drops along the glideslope.

Table 11. Glideslope visibility.

Fig. 5 Path	$\frac{1}{V}$	Visibility
AF	$4.7938 \times 10^{-3} \text{ m}^{-1}$	208.60 m
AC	$9.7194 \times 10^{-3} \text{ m}^{-1}$	102.89 m
AE	$1.4783 \times 10^{-2} \text{ m}^{-1}$	67.65 m

Comparing these visibility values with the values in the right hand column of Table 10 (p. 39) shows that the pilot will be traveling distances which are much longer than the visibility. This indicates that on final approach he would not be able to see the runway until he was approximately 200 m from touchdown.

In this example, as the pilot approaches the ground, his visibility will improve; however, other cases could be proposed that would yield poorer visibility near the surface than at the glideslope entry point aloft. Long glideslopes, small glideslope angles, frequently can make it more difficult to navigate due to poor visibility for a long time on the glideslope.

A situation with low-level stratus clouds and then clear below (greater than 7 km visibility) could also be handled by this drop-size approach. In Fig. 6 the glideslope from E to F may be in the cloud and show a large number of drops with a correspondingly low visibility. The path from F to A would be in the clear sector with the number of drops minimal. Hence, without the dangers of using a laser, it would be possible to predict slant range visibility based on drop-size distribution at several levels.

The visibilities used from Borchers' program in this section appear too low for the existing conditions. However, they were used to demonstrate the feasibility of using changing drop-size distributions with height to forecast slant range visibility and visibility through individual layers. The actual measurement of drop-size distributions at airfields would eliminate the doubt about output of the programs.

5. SUMMARY OF RESULTS

This research has reviewed some of the methods used to obtain visual range and slant visual range. One of these methods, by Davies, was carried further to show that visual range and slant visual range can be obtained during rain by using only the drop-size distribution. This had not been shown specifically in the literature.

In the present research, Capistrano Test Site data (Dickson et al., 1975(a)) were used to show that the complex Mie scattering theory yielded visibilities that were close to reported values by means of a program developed by Kattawar and Plass. Davies' method of computing visibilities from a drop-size distribution was then applied to the same data. The Capistrano data for the 17 April fog case at 0120 hours gave a visibility of 0.500 km. Results from the Kattawar and Plass method gave a lower visibility of 0.421 km and Davies' method showed a higher visibility of 0.541 km. The relatively clear air case at 0120 hours on 18 April gave a visibility of 4.516 km at Capistrano. The Kattawar and Plass method calculated a visibility of 4.452 km and Davies' method a visibility of 5.086 km. The Kattawar and Plass data were not as dependent as the Davies method on the measured drops of small size due to the nature of the program. Some deviation from the reported results was expected since slightly less than 100% of the drops were used in the calculation due to computer run time. The Davies method, however, was slightly restricted because the nephelometer data did not contain all the drops below 3 μm. A comparison of

the results shows that the Davies method gives very good results and can be used to investigate cases of low visibility.

Since no vertical drop-size distributions of rainfall were available, a program developed by Borchers was used to generate a distribution. The Davies method then was applied to his results. The Marshall-Palmer equation was used to obtain a drop-size distribution as a comparison to Borchers' rainfall distribution and resultant visibility. Borchers' surface visibility is compared to the Marshall-Palmer value in Table 12.

Table 12. Comparison of Borchers' surface visibility and the Marshall-Palmer visibility for a rainfall rate of 25 mm/hr.

Radius Range	Borchers' Visibility	Marshall-Palmer Visibility
0.0424-4.3046 mm	208.60 m	--------
0.8542-2.1524 mm	1241.77 m	--------
0.750-2.250 mm in 0.100 mm intervals	----------	644.14 m
0.750-2.250 mm in 0.200 mm intervals	----------	1162.1 m

The Marshall-Palmer result of 1162.1 m and Borchers' 1241.77 m are very close. These were computed over similar radius ranges and radius intervals. This confirmed that Borchers' program is giving acceptable distributions and can be used to investigate slant visual range further.

Slant visual range (glideslope visibility) can be obtained only by using an assumed drop-size distribution. Using Borchers' distribution with height gave the results shown in Table 13.

Table 13. Comparison of slant path visibility to distance flown.

Fig. 6 Path	Slant Path Visibility	Total distance to be flown at 12-deg glideslope
AF (Sfc to 100 m height)	208.60 m	480.97 m
AC (Sfc to 200 m height)	102.89 m	961.95 m
AE (Sfc to 300 m height)	67.65 m	1442.92 m

As can be seen, the pilot will fly a much longer path on the 12-deg glideslope than his visibility will permit him to see. This shows that by using a drop-size distribution for rainfall it is possible to obtain reasonable forecasts of the slant path visibility by Davies' method.

Despite the low visibility values obtained in Borchers' distribution, they were used to verify that Davies' method can be used to calculate visibility over a large radius range along a slant path.

6. CONCLUSIONS

This thesis has shown that visibility measurements have been or can be obtained in various ways from a given drop-size distribution. These included:

1) The use of a fog nephelometer.

2) The use of lidar.

3) The use of Mie scattering theory in a program developed by Kattawar and Plass.

4) The use of an equation proposed by Davies.

A test case from the Capistrano Test Site (Dickson et al., 1975 (a)) was used for fog and damp haze situations. The Marshall-Palmer equation was used to produce a rainfall distribution for various rainfall rates to show the change in visibility that occurs. Finally, a program developed by Borchers in 1979 was used to generate a vertically-varying distribution in rain.

Visibilities were calculated from the numerous data cases. Finally, it was shown that slant visual range also can be calculated by the Davies equation with reasonable results.

Given a drop-size distribution, the Davies method is the most economical one to use in terms of computer time. The Mie theory program was very expensive to run and required large, high-speed computer capability. The use of a lidar would not be inexpensive and poses the hazards mentioned earlier in this work. A nephelometer is safe, but could become costly to use in field instrumentation.

It appears feasible to formulate a set of quick reference tables that could be used to estimate visibility based on selected drop-size distributions. If this is true, airfield personnel should be able to estimate slant range visibility for transiting aircraft. This would definitely improve meteorological support to aircraft.

The ability to have actual experimental drop-size distributions and measured visibilities for various levels and conditions would make possible an in-depth evaluation of the application of Davies' method to the calculation of visibility from drop-size distribution. Possible modifications may need to be applied to the Davies equation to handle different drop ranges and intervals.

7. RECOMMENDATIONS

Several recommendations come to mind:

1) Measure drop-size distribution and visibility in various kinds of weather and at numerous vertical levels.

2) Perform these measurements at various wavelengths to see if there is a favored wavelength for given conditions.

3) Analyze the results in a fashion that will allow multiple comparisons within the data sets.

4) Analyze real conditions to see if the Davies equation requires a variable factor for differing conditions or drop ranges to match consistently the measured results of visibility.

5) Test the viability of using drop-size distributions to obtain slant visual range on a real-time basis. Use weather observers to verify the results.

6) Consider the use of radar to obtain drop-size distributions from a distance. These can be used to estimate precipitation amounts and visibility in the area compared to reported results.

7) Improve current visibility forecasts by integration of drop-size distribution variation in different types of clouds in different parts of the world. This could lead to improved in-flight refueling capability and storm avoidance.

APPENDIX A

Visibility calculations for a 25 mm/hr rainfall rate. Drop-size distribution is for the surface, 100 m, and 200 m from Borchers' program. The first calculation (a) is for the entire distribution and (b) is from 854.2 μm to 2152.4 μm inclusive.

A1) Surface

    (a) $\Sigma \frac{1}{V_i} = 4.7938 \times 10^{-3}$ m^{-1}

        $V = 208.60$ m

    (b) $\Sigma \frac{1}{V_i} = 8.0528 \times 10^{-4}$ m^{-1}

        $V = 1241.77$ m

A2) 100 m

    (a) $\Sigma \frac{1}{V_i} = 4.9256 \times 10^{-3}$ m^{-1}

        $V = 203.02$ m

    (b) $\Sigma \frac{1}{V_i} = 8.1810 \times 10^{-4}$ m^{-1}

        $V = 1222.5$ m

A3) 200 m

    (a) $\Sigma \frac{1}{V_i} = 5.0639 \times 10^{-3}$ m^{-1}

        $V = 197.48$ m

    (b) $\Sigma \frac{1}{V_i} = 8.3077 \times 10^{-4}$ m^{-1}

        $V = 1203.8$ m

Table A1. Values used in Davies' equation for Borchers' program data at the surface.

Radius[a]	$n(r)$[b]	$n(r)r_i^{2c}$	E_i	$n_i r_i^2 E_i^c$	$\frac{1}{V_i}$ d
42.4	1.0835×10^4	1.9479×10^1	2.0	3.8957×10^1	3.1382×10^{-5}
47.6	1.1210×10^4	2.5399×10^1	2.0	5.0798×10^1	4.0920×10^{-5}
53.4	1.0095×10^4	2.8786×10^1	2.0	5.7573×10^1	4.6377×10^{-5}
59.9	8.8400×10^3	3.1718×10^1	2.0	6.3436×10^1	5.1100×10^{-5}
67.3	7.8800×10^3	3.5691×10^1	2.0	7.1382×10^1	5.7500×10^{-5}
75.5	7.0850×10^3	4.0386×10^1	2.0	8.0773×10^1	6.5065×10^{-5}
84.8	6.4200×10^3	4.6166×10^1	2.0	9.2333×10^1	7.4378×10^{-5}
95.1	5.8450×10^3	5.2862×10^1	2.0	1.0572×10^2	8.5165×10^{-5}
105.8	5.3150×10^3	6.0624×10^1	2.0	1.2125×10^2	9.7670×10^{-5}
119.9	4.8275×10^3	6.9400×10^1	2.0	1.3880×10^2	1.1181×10^{-4}
134.5	4.3725×10^3	7.9100×10^1	2.0	1.5820×10^2	1.2744×10^{-4}
151.0	3.9295×10^3	8.9597×10^1	2.0	1.7919×10^2	1.4435×10^{-4}

Table A1. Continued.

Radius[a]	$n(r)$[b]	$n(r)r_i^2$[c]	E_i	$n_i r_i^2 E_i$[c]	$\frac{1}{V_i}$[d]
169.5	3.4070×10^3	9.7884×10^1	2.0	1.9577×10^2	1.5770×10^{-4}
190.3	2.9960×10^3	1.0850×10^2	2.0	2.1699×10^2	1.7480×10^{-4}
213.6	2.5785×10^3	1.1764×10^2	2.0	2.3529×10^2	1.8953×10^{-4}
239.7	2.2010×10^3	1.2646×10^2	2.0	2.5292×10^2	2.0374×10^{-4}
269.1	1.8540×10^3	1.3426×10^2	2.0	2.6851×10^2	2.1630×10^{-4}
302.0	1.5465×10^2	1.4105×10^2	2.0	2.8209×10^2	2.2724×10^{-4}
339.0	1.2735×10^3	1.4635×10^2	2.0	2.9270×10^2	2.3578×10^{-4}
380.5	1.0365×10^3	1.5006×10^2	2.0	3.0013×10^2	2.4177×10^{-4}
427.1	8.3550×10^2	1.5241×10^2	2.0	3.0481×10^2	2.4554×10^{-4}
479.4	6.6500×10^2	1.5283×10^2	2.0	3.0567×10^2	2.4623×10^{-4}
538.1	5.1950×10^2	1.5042×10^2	2.0	3.0084×10^2	2.4234×10^{-4}
604.0	3.9805×10^2	1.4522×10^2	2.0	2.9043×10^2	2.3395×10^{-4}

Table A1. Continued.

Radius[a]	$n(r)$[b]	$n(r)r_i^2$[c]	E_i	$n_i r_i^2 E_i$[c]	$\frac{1}{V_i}$[d]
678.0	2.9810×10^2	1.3703×10^2	2.0	2.7406×10^2	2.2077×10^{-4}
761.0	2.1765×10^2	1.2605×10^2	2.0	2.5209×10^2	2.0307×10^{-4}
* 854.2	1.5465×10^2	1.1284×10^2	2.0	2.2568×10^2	1.8180×10^{-4}
* 958.8	1.0630×10^2	9.7721×10^1	2.0	1.9544×10^2	1.5744×10^{-4}
* 1076.2	7.0500×10^1	8.1654×10^1	2.0	1.6331×10^2	1.3155×10^{-4}
* 1208.0	4.5015×10^1	6.5689×10^1	2.0	1.3138×10^2	1.0583×10^{-4}
* 1355.9	2.7505×10^1	5.0567×10^1	2.0	1.0113×10^2	8.1467×10^{-5}
* 1522.0	1.6065×10^1	3.7214×10^1	2.0	7.4429×10^1	5.9955×10^{-5}
* 1708.4	8.9300	2.6063×10^1	2.0	5.2127×10^1	4.1990×10^{-5}
* 1917.6	4.7070	1.7309×10^1	2.0	3.4617×10^1	2.7885×10^{-5}
* 2152.4	2.3270	1.0781×10^1	2.0	2.1561×10^1	1.7368×10^{-5}
2416.0	1.0485	6.1202	2.0	1.2240×10^1	9.8600×10^{-6}

Table A1. Continued.

Radius[a]	$n(r)$[b]	$n(r)r_i^{2c}$	E_i	$n_i r_i^2 E_i^c$	$\frac{1}{V_i}$[d]
2711.8	4.0350×10^{-1}	2.9673	2.0	5.9346	4.7805×10^{-6}
3043.9	1.1050×10^{-1}	1.0238	2.0	2.0476	1.6494×10^{-6}
3416.6	1.6145×10^{-2}	1.8846×10^{-1}	2.0	3.7693×10^{-1}	3.0363×10^{-7}
3635.0	1.2325×10^{-3}	1.8127×10^{-2}	2.0	3.6253×10^{-2}	2.9203×10^{-8}
4304.6	1.2975×10^{-4}	2.4042×10^{-3}	2.0	4.8084×10^{-3}	3.8734×10^{-9}
4831.8	0.0	0.0	2.0	0.0	0.0

$\Sigma n(r) = 1.0692 \times 10^5$

$*\Sigma n(r) = 4.3600 \times 10^2$

$\Sigma \frac{1}{V_i} = 4.7938 \times 10^{-3} \text{ m}^{-1}$

$*\Sigma \frac{1}{V_i} = 8.0528 \times 10^{-4} \text{ m}^{-1}$

a Units in microns.
b Number of drops/m³.
c Number of drops/m.
d m⁻¹.

Table A2. Values used in Davies' equation for Borchers' program data at the 100-m level.

Radius[a]	$n(r)$[b]	$n(r)r_i^2$[c]	E_i	$n_i r_i^2 E_i$[c]	$\frac{1}{V_i}$[d]
42.4	1.1510×10^4	2.0692×10^1	2.0	4.1394×10^1	3.3337×10^{-5}
47.6	1.1895×10^4	2.6951×10^1	2.0	5.3902×10^1	4.3420×10^{-5}
53.4	1.0735×10^4	3.0611×10^1	2.0	6.1223×10^1	4.9317×10^{-5}
59.9	9.3750×10^3	3.3638×10^1	2.0	6.7275×10^1	5.4193×10^{-5}
67.3	8.3250×10^3	3.7706×10^1	2.0	7.5413×10^1	6.0748×10^{-5}
75.5	7.4650×10^3	4.2552×10^1	2.0	8.5105×10^1	6.8555×10^{-5}
84.8	6.7450×10^3	4.8504×10^1	2.0	9.7007×10^1	7.8143×10^{-5}
95.1	6.1250×10^3	5.5395×10^1	2.0	1.1079×10^1	8.9245×10^{-5}
106.8	5.5550×10^3	6.3362×10^1	2.0	1.2672×10^2	1.0208×10^{-4}
119.9	5.0350×10^3	7.2383×10^1	2.0	1.4477×10^2	1.1661×10^{-4}
134.5	4.5485×10^3	8.2284×10^1	2.0	1.6457×10^2	1.3256×10^{-4}
151.0	4.0770×10^3	9.2960×10^1	2.0	1.8592×10^2	1.4976×10^{-4}

Table A2. Continued.

Radius[a]	$n(r)$[b]	$n(r)r_i^2$[c]	E_i	$n_i r_i^2 E_i$[c]	$\frac{1}{V_i}$[d]
169.5	3.5245×10^3	1.0126×10^2	2.0	2.0252×10^2	1.6314×10^{-4}
190.3	3.0910×10^3	1.1194×10^2	2.0	2.2388×10^2	1.8034×10^{-4}
213.6	2.6530×10^3	1.2104×10^2	2.0	2.4209×10^2	1.9501×10^{-4}
239.7	2.2595×10^3	1.2982×10^2	2.0	2.5964×10^2	2.0915×10^{-4}
269.1	1.8995×10^3	1.3755×10^2	2.0	2.7510×10^2	2.2161×10^{-4}
302.0	1.5820×10^3	1.4428×10^2	2.0	2.8857×10^2	2.3245×10^{-4}
339.0	1.3020×10^3	1.4963×10^2	2.0	2.9925×10^2	2.4106×10^{-4}
380.5	1.0590×10^3	1.5332×10^2	2.0	3.0664×10^2	2.4701×10^{-4}
427.1	8.5400×10^2	1.5578×10^2	2.0	3.1156×10^2	2.5098×10^{-4}
479.4	6.7950×10^2	1.5617×10^2	2.0	3.1233×10^2	2.5159×10^{-4}
538.1	5.3150×10^2	1.5390×10^2	2.0	3.0779×10^2	2.4794×10^{-4}
604.0	4.0705×10^2	1.4850×10^2	2.0	2.9700×10^2	2.3924×10^{-4}

Table A2. Continued.

Radius[a]	$n(r)$[b]	$n(r)r_i^2$[c]	E_i	$n_i r_i^2 E_i$[c]	$\frac{1}{V_i}$[d]
678.0	3.0485×10^2	1.4013×10^2	2.0	2.8027×10^2	2.2577×10^{-4}
761.0	2.2250×10^2	1.2885×10^2	2.0	2.5771×10^2	2.0759×10^{-4}
* 854.2	1.5800×10^2	1.1529×10^2	2.0	2.3057×10^2	1.8573×10^{-4}
* 958.8	1.0845×10^2	9.9698×10^1	2.0	1.9940×10^2	1.6062×10^{-4}
* 1076.2	7.1750×10^1	8.3101×10^1	2.0	1.6620×10^2	1.3388×10^{-4}
* 1208.0	4.5700×10^1	6.6688×10^1	2.0	1.3338×10^2	1.0744×10^{-4}
* 1355.9	2.7835×10^1	5.1174×10^1	2.0	1.0235×10^2	8.2445×10^{-5}
* 1522.0	1.6200×10^1	3.7527×10^1	2.0	7.5054×10^1	6.0459×10^{-5}
* 1708.4	8.9800	2.6209×10^1	2.0	5.2419×10^1	4.2225×10^{-5}
* 1917.6	4.7160	1.7342×10^1	2.0	3.4683×10^1	2.7939×10^{-5}
* 2152.4	2.3265	1.0778×10^1	2.0	2.1557×10^1	1.7365×10^{-5}
2416.0	1.0490	6.1231	2.0	1.2246×10^1	9.8647×10^{-6}

Table A2. Continued.

Radius[a]	$n(r)$[b]	$n(r)r_i^{2c}$	E_i	$n_i r_i^2 E_i^c$	$\frac{1}{V_i}$[d]
2711.8	4.0560×10^{-1}	2.9827	2.0	5.9655	4.8054×10^{-6}
3043.9	1.1240×10^{-1}	1.0414	2.0	2.0828	1.6778×10^{-6}
3416.6	1.6580×10^{-2}	1.9354×10^{-1}	2.0	3.8708×10^{-1}	3.1181×10^{-7}
3835.0	1.2645×10^{-3}	1.8597×10^{-2}	2.0	3.7195×10^{-2}	2.9962×10^{-8}
4304.6	1.3320×10^{-5}	2.4681×10^{-4}	2.0	4.9363×10^{-4}	3.9764×10^{-10}
4831.8	0.0	0.0	2.0	0.0	0.0

$\Sigma \frac{1}{V_i} = 4.9256 \times 10^{-3} \text{ m}^{-1}$

$*\Sigma \frac{1}{V_i} = 8.1810 \times 10^{-4} \text{ m}^{-1}$

$\Sigma n(r) = 1.1221 \times 10^5$

$*\Sigma n(r) = 4.4396 \times 10^2$

a Units in microns.
b Number of drops/m^3.
c Number of drops/m.
d m^{-1}.

Table A3. Values used in Davies' equation for Borchers' program data at the 200-m level.

Radius[a]	$n(r)$[b]	$n(r)r_i^2$[c]	E_i	$n(r)r_i^2E_i$[c]	$\frac{1}{V_i}$[d]
42.4	1.2300×10^4	2.2112×10^1	2.0	4.4225×10^1	3.5625×10^{-5}
47.6	1.2685×10^4	2.8741×10^1	2.0	5.7482×10^1	4.6304×10^{-5}
53.4	1.1475×10^4	3.2722×10^1	2.0	6.5443×10^1	5.2717×10^{-5}
59.9	9.9800×10^3	3.5808×10^1	2.0	7.1617×10^1	5.7690×10^{-5}
67.3	8.3400×10^3	4.0035×10^1	2.0	8.0078×10^1	6.4506×10^{-5}
75.5	7.9000×10^3	4.5032×10^1	2.0	9.0064×10^1	7.2550×10^{-5}
84.8	7.1150×10^3	5.1164×10^1	2.0	1.0233×10^2	8.2429×10^{-5}
95.1	6.4400×10^3	5.8243×10^1	2.0	1.1649×10^2	9.3834×10^{-5}
106.8	5.8250×10^3	6.6441×10^1	2.0	1.3288×10^2	1.0704×10^{-4}
119.9	5.2650×10^3	7.5690×10^1	2.0	1.5138×10^2	1.2194×10^{-4}
134.5	4.7425×10^3	8.5793×10^1	2.0	1.7159×10^2	1.3822×10^{-4}
151.0	4.2380×10^3	9.6631×10^1	2.0	1.9326×10^2	1.5568×10^{-4}

Table A3. Continued.

Radius[a]	$n(r)$[b]	$n(r)r_i^2$[c]	E_i[b]	$n(r)r_i^2 E_i$[c]	$\frac{1}{V_i}$[d]
169.5	3.6515×10^3	1.0491×10^2	2.0	2.0982×10^2	1.6902×10^{-4}
190.3	3.1925×10^3	1.1561×10^2	2.0	2.3123×10^2	1.8626×10^{-4}
213.6	2.7320×10^3	1.2465×10^2	2.0	2.4929×10^2	2.0082×10^{-4}
239.7	2.3205×10^3	1.3333×10^2	2.0	2.6665×10^2	2.1480×10^{-4}
269.1	1.9475×10^3	1.4103×10^2	2.0	2.8206×10^2	2.2721×10^{-4}
302.0	1.6195×10^3	1.4770×10^2	2.0	2.9541×10^2	2.3796×10^{-4}
339.0	1.3320×10^3	1.5082×10^2	2.0	3.0163×10^2	2.4298×10^{-4}
380.5	1.0825×10^3	1.5672×10^2	2.0	3.1345×10^2	2.5249×10^{-4}
427.1	8.7300×10^2	1.5925×10^2	2.0	3.1850×10^2	2.5656×10^{-4}
579.4	6.9550×10^2	1.5984×10^2	2.0	3.1969×10^2	2.5752×10^{-4}
538.1	5.4400×10^2	1.5752×10^2	2.0	3.1503×10^2	2.5377×10^{-4}
604.0	4.1670×10^2	1.5202×10^2	2.0	3.0404×10^2	2.4491×10^{-4}

Table A3. Continued.

Radius[a]	$n(r)$[b]	$n(r)r_i^2$[c]	E_i	$n(r)r_i^2E_i$[c]	$\frac{1}{V_i}$[d]
678.0	3.1210×10^2	1.4347×10^2	2.0	2.8693×10^2	2.3114×10^{-4}
761.0	2.2770×10^2	1.3187×10^2	2.0	2.6373×10^2	2.1245×10^{-4}
*854.2	1.6150×10^2	1.1784×10^2	2.0	2.3568×10^2	1.8985×10^{-4}
*958.8	1.1065×10^2	1.0172×10^2	2.0	2.0344×10^2	1.6388×10^{-4}
*1076.2	7.3050×10^1	8.4607×10^1	2.0	1.6921×10^2	1.3631×10^{-4}
*1208.0	4.6365×10^1	6.7659×10^1	2.0	1.3532×10^2	1.0900×10^{-4}
*1355.9	2.8140×10^1	5.1734×10^1	2.0	1.0347×10^2	8.3348×10^{-5}
*1522.0	1.6310×10^1	3.7782×10^1	2.0	7.5564×10^1	6.0869×10^{-5}
*1708.4	9.0000	2.6268×10^1	2.0	5.2535×10^1	4.2319×10^{-5}
*1917.6	4.7095	1.7318×10^1	2.0	3.4635×10^1	2.7900×10^{-5}
*2152.4	2.3175	1.0737×10^1	2.0	2.1473×10^1	1.7297×10^{-5}
2416.0	1.0450	6.0997	2.0	1.2199×10^1	9.8271×10^{-6}

Table A3. Continued.

Radius[a]	$n(r)$[b]	$n(r)r_i^2$[c]	E_i	$n(r)r_i^2 E_i$[c]	$\frac{1}{V_i}$[d]
2711.8	4.0595×10^{-1}	2.9853	2.0	5.9706	4.8095×10^{-6}
3043.9	1.1400×10^{-1}	1.0562	2.0	2.1125	1.7017×10^{-6}
3416.6	1.7010×10^{-2}	1.9856×10^{-1}	2.0	3.9712×10^{-1}	3.1990×10^{-7}
3835.0	1.2960×10^{-3}	1.9061×10^{-2}	2.0	3.8121×10^{-2}	3.0708×10^{-7}
4304.6	1.3650×10^{-4}	2.5293×10^{-3}	2.0	5.0586×10^{-3}	4.0749×10^{-9}
4831.8	0.0	0.0	2.0	0.0	0.0

$\Sigma n(r) = 1.1821 \times 10^5$

$*\Sigma n(r) = 4.5204 \times 10^2$

$\Sigma \frac{1}{V_i} = 5.0639 \times 10^{-3} \ m^{-1}$

$*\Sigma \frac{1}{V_i} = 8.3077 \times 10^{-4} \ m^{-1}$

a Units in microns.
b Number of drops/m^3.
c Number of drops/m.
d m^{-1}.

APPENDIX B

Visibility calculations for the rainfall rates of 5, 12, 25, 50, and 100 mm/hr using the Marshall-Palmer distribution and a radius interval of 0.100 mm.

1) 5 mm/hr

$$\Sigma \frac{1}{V_i} = 4.3896 \times 10^{-4} \ m^{-1}$$

$$V = 2278.1 \ m$$

2) 12 mm/hr

$$\Sigma \frac{1}{V_i} = 7.5324 \times 10^{-4} \ m^{-1}$$

$$V = 1327.6 \ m$$

3) 25 mm/hr

$$\Sigma \frac{1}{V_i} = 1.5525 \times 10^{-3} \ m^{-1}$$

$$V = 644.1 \ m$$

4) 50 mm/hr

$$\Sigma \frac{1}{V_i} = 2.8939 \times 10^{-3} \ m^{-1}$$

$$V = 345.6 \ m$$

5) 100 mm/hr

$$\Sigma \frac{1}{V_i} = 5.1161 \times 10^{-3} \ m^{-1}$$

$$V = 195.5 \ m$$

Table B1. Values used in Davies' equation for a Marshall-Palmer distribution at 5 mm/hr rainfall rate.

Radius[a]	$n(r)$[b]	$n(r)r_i^{2}$[c]	E_i	$n(r)r_i^{2}E_i$[c]	$\frac{1}{\bar{V}_i}$[d]
* 0.625	2.0685×10^{2}	8.0802×10^{1}	2.0	1.6160×10^{2}	1.3018×10^{-4}
0.675	1.5441×10^{2}	7.0352×10^{1}	2.0	1.4070×10^{2}	1.1334×10^{-4}
* 0.725	1.1526×10^{2}	6.0583×10^{1}	2.0	1.2117×10^{2}	9.7603×10^{-5}
0.775	8.6035×10^{1}	5.1675×10^{1}	2.0	1.0335×10^{2}	8.3252×10^{-5}
* 0.825	6.4222×10^{1}	4.3711×10^{1}	2.0	8.7422×10^{1}	7.0422×10^{-5}
0.875	4.7939×10^{1}	3.6703×10^{1}	2.0	7.3407×10^{1}	5.9132×10^{-5}
* 0.925	3.5784×10^{1}	3.0618×10^{1}	2.0	6.1236×10^{1}	4.9328×10^{-5}
0.975	2.6712×10^{1}	2.5393×10^{1}	2.0	5.0785×10^{1}	4.0910×10^{-5}
* 1.025	1.9939×10^{1}	2.0949×10^{1}	2.0	4.1897×10^{1}	3.3750×10^{-5}
1.075	1.4894×10^{1}	1.7200×10^{1}	2.0	3.4400×10^{1}	2.7710×10^{-5}
* 1.125	1.1110×10^{1}	1.4061×10^{1}	2.0	2.8122×10^{1}	2.2654×10^{-5}
1.175	8.2932	1.1450×10^{1}	2.0	2.2900×10^{1}	1.8446×10^{-5}

Table B1. Continued.

Radius[a]	$n(r)$[b]	$n(r)r_i^2$[c]	E_i	$n(r)r_i^2E_i$[c]	$\dfrac{1}{V_i}$[d]
* 1.225	6.1905	9.2897	2.0	1.8579×10^1	1.4966×10^{-5}
1.275	4.6210	7.5120	2.0	1.5024×10^1	1.2102×10^{-5}
* 1.325	3.4494	6.0558	2.0	1.2112×10^1	9.7563×10^{-6}
1.375	2.7548	4.8680	2.0	9.7360	7.8427×10^{-6}
* 1.425	1.9220	3.9028	2.0	7.8057	6.2878×10^{-6}
1.475	1.4347	3.1213	2.0	6.2427	5.0287×10^{-6}
1.500	1.2395	2.7890	2.0	5.5779	4.4932×10^{-6}
* 1.525	1.0709	2.4906	2.0	4.9812	4.0125×10^{-6}

$\Sigma n(r) = 1.2189 \times 10^3$

$^*\Sigma n(r) = 4.6580 \times 10^2$

$^*\Sigma \dfrac{1}{V_i} = 4.3896 \times 10^{-4} \ m^{-1}$

a Units in millimeters.
b Number of drops/m³.
c Number of drops/m.
d m⁻¹.

Table B2. Values used in Davies' equation for a Marshall-Palmer distribution at 12 mm/hr rainfall rate.

Radius[a]	$n(r)$[b]	$n(r)r_i^2$[c]	E_i	$n(r)r_i^2E_i$[c]	$\frac{1}{V_i}$[d]
0.750	2.0801×10^2	1.1701×10^2	2.0	2.3401×10^2	1.8850×10^{-4}
0.850	1.2786×10^2	9.2382×10^1	2.0	1.8476×10^2	1.4883×10^{-4}
0.950	7.8598×10^1	7.0935×10^1	2.0	1.4187×10^2	1.1428×10^{-4}
1.050	4.8315×10^1	5.3267×10^1	2.0	1.0653×10^2	8.5817×10^{-5}
1.150	2.9699×10^1	3.9277×10^1	2.0	7.8554×10^1	6.3278×10^{-5}
1.250	1.8256×10^1	2.8525×10^1	2.0	5.7051×10^1	4.5956×10^{-5}
1.350	1.1222×10^1	2.0452×10^1	2.0	4.0905×10^1	3.2950×10^{-5}
1.450	6.8983	1.4504×10^1	2.0	2.9007×10^1	2.3366×10^{-5}
1.550	4.2404	1.0188×10^1	2.0	2.0375×10^1	1.6413×10^{-5}
1.650	2.6066	7.0964	2.0	1.4193×10^1	1.1433×10^{-5}
1.750	1.6023	4.9070	2.0	9.8140	7.9055×10^{-6}

Table B2. Continued.

Radius[a]	$n(r)$[b]	$n(r)r_i^2$[c]	E_i	$n(r)r_i^2 E_i$[c]	$\frac{1}{V_i}$[d]
1.850	9.8493×10^{-1}	3.3709	2.0	6.7418	5.4308×10^{-6}
1.950	6.0544×10^{-1}	2.3022	2.0	4.6044	3.7090×10^{-6}
2.050	3.7217×10^{-1}	1.5640	2.0	3.1280	2.5198×10^{-6}
2.150	2.2877×10^{-1}	1.0575	2.0	2.1150	1.7037×10^{-6}
2.250	1.0463×10^{-1}	7.1192×10^{-1}	2.0	1.4238	1.1470×10^{-5}

$\Sigma n(r) = 5.3660 \times 10^2$

$\Sigma \frac{1}{V_i} = 7.5324 \times 10^{-4}\ m^{-1}$

a Units in millimeters.
b Number of drops/m^3.
c Number of drops/m.
d m^{-1}.

Table B3. Values used in Davies' equation for a Marshall-Palmer distribution at 25 mm/hr rainfall rate.

Radius[a]	$n(r)$[b]	$n(r)r_i^2$[c]	E_i	$n(r)r_i^2E_i$[c]	$\frac{i}{V_i}$[d]
0.750	3.5034×10^2	1.9707×10^2	2.0	3.9413×10^2	3.1749×10^{-4}
0.850	2.3086×10^2	1.6680×10^2	2.0	3.3359×10^2	2.6872×10^{-4}
0.950	1.5212×10^2	1.3729×10^2	2.0	2.7458×10^2	2.2118×10^{-4}
1.050	1.0024×10^2	1.1051×10^2	2.0	2.2103×10^2	1.7805×10^{-4}
1.150	6.6054×10^1	8.7357×10^1	2.0	1.7471×10^2	1.4074×10^{-4}
1.250	4.3527×10^1	6.8010×10^1	2.0	1.3602×10^2	1.0957×10^{-4}
1.350	2.8682×10^1	5.2273×10^1	2.0	1.0455×10^2	8.4215×10^{-5}
1.450	1.8900×10^1	3.9737×10^1	2.0	7.9474×10^1	6.4019×10^{-5}
1.550	1.2454×10^1	2.9921×10^1	2.0	5.9842×10^1	4.8205×10^{-5}
1.650	8.2067	2.2343×10^1	2.0	4.4685×10^1	3.5996×10^{-5}
1.750	5.4078	1.6561×10^1	2.0	3.3123×10^1	2.6682×10^{-5}

Table B3. Continued.

Radius[a]	$n(r)$[b]	$n(r)r_i^2$[c]	E_i	$n(r)r_i^2 E_i$[c]	$\frac{1}{V_i}$[d]
1.850	3.5635	1.2196×10^1	2.0	2.4392×10^1	1.9649×10^{-5}
1.950	2.3482	8.9289	2.0	1.7858×10^1	1.4385×10^{-5}
2.050	1.5473	6.5026	2.0	1.3005×10^1	1.0476×10^{-5}
2.150	1.0195	4.7131	2.0	9.4263	7.5932×10^{-6}
2.250	6.7187×10^{-1}	3.4013	2.0	6.8027	5.4798×10^{-6}

$\Sigma n(r) = 1.0259 \times 10^3$

$\Sigma \frac{1}{V_i} = 1.5525 \times 10^{-3}\ m^{-1}$

a Units in millimeters.
b Number of drops/m^3.
c Number of drops/m.
d m^{-1}.

Table B4. Values used in Davies' equation for a Marshall-Palmer distribution at 50 mm/hr rainfall rate.

Radius[a]	n(r)[b]	$n(r)r_i^2$ [c]	E_i	$n(r)r_i^2E_i$ [c]	$\frac{1}{V_i}$ [d]
0.750	5.3522×10^2	3.0106×10^2	2.0	6.0212×10^2	4.8503×10^{-4}
0.850	3.7318×10^2	2.6962×10^2	2.0	5.3925×10^2	4.3438×10^{-4}
0.950	2.6020×10^2	2.3483×10^2	2.0	4.6967×10^2	3.7833×10^{-4}
1.050	1.8143×10^2	2.0002×10^2	2.0	4.0005×10^2	3.2225×10^{-4}
1.150	1.2650×10^2	1.6730×10^2	2.0	3.3460×10^2	2.6953×10^{-4}
1.250	8.8204×10^1	1.3782×10^2	2.0	2.7564×10^2	2.2204×10^{-4}
1.350	6.1501×10^1	1.1208×10^2	2.0	2.2417×10^2	1.8058×10^{-4}
1.450	4.2882×10^1	9.0159×10^1	2.0	1.8032×10^2	1.4525×10^{-4}
1.550	2.9899×10^1	7.1833×10^1	2.0	1.4367×10^2	1.1573×10^{-4}
1.650	2.0848×10^1	5.6757×10^1	2.0	1.1351×10^2	9.1440×10^{-5}
1.750	1.4536×10^1	4.4517×10^1	2.0	8.9033×10^1	7.1720×10^{-5}

Table B4. Continued.

Radius[a]	$n(r)$[b]	$n(r)r_i^2$[c]	E_i	$n(r)r_i^2E_i$[c]	$\frac{1}{V_i}$[d]
1.850	1.0135×10^1	3.4688×10^1	2.0	6.9376×10^1	5.5885×10^{-5}
1.950	7.0669	2.6872×10^1	2.0	5.3744×10^1	4.3293×10^{-5}
2.050	4.9274	2.0708×10^1	2.0	4.1415×10^1	3.3361×10^{-5}
2.150	3.4357	1.5881×10^1	2.0	3.1763×10^1	2.5586×10^{-5}
2.250	2.3956	1.2127×10^1	2.0	2.4255×10^1	1.9538×10^{-5}

$\Sigma n(r) = 1.7624 \times 10^3$

$$\Sigma \frac{1}{V_i} = 2.8939 \times 10^{-3} \text{ m}^{-1}$$

a Units in millimeters.
b Number of drops/m³.
c Number of drops/m.
d m⁻¹.

Table B5. Values used in Davies' equation for a Marshall-Palmer distribution at 100 mm/hr rainfall rate.

Radius[a]	$n(r)$[b]	$n(r)r_i^2$[c]	E_i	$n(r)r_i^2 E_i$[c]	$\frac{1}{V_i}$[d]
0.750	7.7204×10^2	4.3427×10^2	2.0	8.6854×10^2	6.9964×10^{-4}
0.850	5.6525×10^2	4.0846×10^2	2.0	8.1679×10^2	6.5796×10^{-4}
0.950	4.1386×10^2	3.7351×10^2	2.0	7.4701×10^2	6.0175×10^{-4}
1.050	3.0301×10^2	3.3407×10^2	2.0	6.6814×10^2	5.3821×10^{-4}
1.150	2.2185×10^2	2.9340×10^2	2.0	5.8680×10^2	4.7269×10^{-4}
1.250	1.6243×10^2	2.5380×10^2	2.0	5.0760×10^2	4.0889×10^{-4}
1.350	1.1893×10^2	2.1674×10^2	2.0	4.3348×10^2	3.4919×10^{-4}
1.450	8.7073×10^1	1.8307×10^2	2.0	3.6614×10^2	2.9494×10^{-4}
1.550	6.3751×10^1	1.5316×10^2	2.0	3.0633×10^2	2.4676×10^{-4}
1.650	4.6676×10^1	1.2708×10^2	2.0	2.5415×10^2	2.0473×10^{-4}
1.750	3.4174×10^1	1.0466×10^2	2.0	2.0932×10^2	1.6861×10^{-4}

Table B5. Continued.

Radius[a]	$n(r)$ [b]	$n(r)r_i^2$ [c]	E_i	$n(r)r_i^2 E_i$ [c]	$\frac{1}{V_i}$ [d]
1.850	2.5021×10^1	8.5635×10^1	2.0	1.7127×10^2	1.3796×10^{-4}
1.950	1.8320×10^1	6.9660×10^1	2.0	1.3932×10^2	1.1223×10^{-4}
2.050	1.3413×10^1	5.6367×10^1	2.0	1.1273×10^2	9.0812×10^{-5}
2.150	9.8204	4.5395×10^1	2.0	9.0789×10^1	7.3134×10^{-5}
2.250	7.1901	3.6400×10^1	2.0	7.2800×10^1	5.8643×10^{-5}

$\Sigma n(r) = 2.8628 \times 10^3$

$\Sigma \frac{1}{V_i} = 5.1161 \times 10^{-3} \ m^{-1}$

a Units in millimeters.
b Number of drops/m^3.
c Number of drops/m.
d m^{-1}.

REFERENCES

Bertolotti, M., L. Muzii and D. Sette, 1969: On the possibility of measuring optical visibility by using a ruby laser. _Appl. Opt._, 8, 117-120.

Borchers, R., 1979: Drop distribution program. Personal communication. Headquarters AWS/SY, Scott AFB, IL 62225.

Burke, S. L., 1979: Meteorological studies. AFGL-TR-79-0047, Air Force Geophysics Laboratory, 185 pp. (AD A067937)

Chandrasekhar, S., 1960: _Radiative Transfer_. Dover Publications, Inc., 393 pp.

Davies, C. N., 1975: Visual range and size of atmospheric particles. _J. Aerosol Sci._, 6, 335-347.

Dickson, D. H., R. B. Loveland and W. H. Hatch, 1975(a): Atmospheric waterdrop size distribution at Capistrano Test Site (CTS) from 16 April through 11 May 1974. Vol. I ECOM-DR-75-3-Vol-1, Atmospheric Sciences Laboratory, US Army Electronics Command, 13 pp. (AD A031089)

_____, _____ and _____, 1975(b): Atmospheric waterdrop size distribution at Capistrano Test Site (CTS) from 16 April through 11 May 1974. Vol. II ECOM-DR-75-3-Vol-2, Atmospheric Sciences Laboratory, US Army Electronics Command, 312 pp. (AD A032869)

Diermendjian, D., 1969: _Electromagnetic Scattering on Spherical Polydispersions_. American Elsevier Publishing Company, Inc., 290 pp.

Fenn, R. W., 1966: Correlation between atmospheric backscattering and meteorological visual range. _Appl. Opt._, 5, 293-295.

Fernald, F. G., R. J. Allen, J. Oblanas, R. T. H. Collis, M. G. H. Ligda and R. G. Hadfield, 1967: Use of lidar in support of Point Mugu Range Operations. Stanford Research Institute, 73 pp. (AD 923606)

Ferrara, R., G. Fiocco and G. Tonna, 1970: Evolution of the fog droplet size distribution observed by laser scattering. Appl. Opt., 9, 2517-2521.

Folster, H., D. H. Dickson and R. B. Loveland, 1975: A lasar fog nephelometer: Its description, calibration, and field testing. Third Symposium on Meteorological Observations and Instrumentation, Washington, D.C., Amer. Meteor. Soc., 61-64.

Hering, W. S., and E. B. Geisler, 1978: Forward scatter meter measurements of slant visual range. AFGL-TR-78-0191, 28 pp. (AD A064429)

Houghton, H. G., and W. R. Chalker, 1949: The scattering cross section of water drops in air for visible light. J. Opt. Soc. Am., 39, 955-957.

Kattawar, G. W., and G. N. Plass, 1968: Influence of particle size distribution on reflected and transmitted light from clouds. Appl. Opt., 7, 869-878.

Lewis, W., 1978: Comparison of slant and runway visual range relationships for 100, 124, and 155 feet. FAA-RD-77-191, Federal Aviation Adminstration, 12 pp. (AD 052870)

Lewis, W., and E. E. Schlatter, 1977: Slant and runway visual range relationships. FAA-RD-77-34, Federal Aviation Administration, 30 pp. (AD 041134)

Lifsitz, J. R., 1974(a): The measurement of atmospheric visibility with lidar: TSC field test results. FAA-RD-74-29, Transportation Systems Center, 114 pp. (AD 777533)

_____, 1974(b): Lidar systems for measuring visibility. A technical assessment. FAA-RD-74-149, Transportation Systems Center, 50 pp. (AD/A-001565)

List, R. J., 1966: Smithsonian Meteorological Tables, Sixth Revised Edition. Smithsonian Institution, 527 pp.

Mason, B. J., 1971: The Physics of Clouds. second edition. Clarendon Press, 671 pp.

McCartney, E. J., 1976: Optics of the Atmosphere: Scattering by Molecules and Particles. John Wiley & Sons, 408 pp.

Meyer, M. B., J. E. Jiusto and G. G. Lala, 1980: Measurements of visual range and radiation-fog (haze) microphysics. J. Atm. Sci., 37, 622-629.

Middleton, W. E. K., 1952: Vision Through the Atmosphere. University of Toronto Press, 250 pp.

Moller, F., 1964: Optics of the lower atmosphere. Appl. Opt., 3, 157-166.

Mooradian, G. E., M. Geller, L. B. Stotts, D. H. Stephens and R. A. Krautwald, 1979: Blue-green pulsed propagation through fog. Appl. Opt., 18, 429-441.

Moroz, E. Y., 1977: Investigation of sensors and techniques to automate weather observations. AFGL-TR-77-0041, Air Force Geophysics Laboratory, 17 pp. (AD A040747)

Moyer, V. E., 1976: Notes on Physical Meteorology. Texas A&M
    University, 236 pp.

Newcomb, F. R., 1972: On the feasibility of determining slant-range
    visibility by using measurements of scattered light. Thesis,
    Texas A&M University, College Station, 60 pp.

Nilsson, B., 1979: Meteorological influence on aerosol extinction
    in the 0.2-40-μm wavelength range. Appl. Opt., 18, 3457-3473.

Plass, G. N., and G. W. Kattawar, 1968: Monte Carlo calculations of
    light scattering from clouds. Appl. Opt., 7, 415-419.

_____, and _____, 1971: Reflection of light pulses from clouds.
    Appl. Opt., 10, 2304-2310.

Preisendorfer, R. W., 1976(a): Hydrologic Optics: Vol I.
    Introduction. U.S. Department of Commerce, 218 pp.

_____, 1976(b): Hydrologic Optics: Vol II. Foundations.
    U.S. Department of Commerce, 400 pp.

Pruppacher, H. R. and J. D. Klett, 1978: Microphysics of Clouds and
    Precipitation. D. Reidel Publishing Company, 714 pp.

Twomey, S., and H. B. Howell, 1965: The relative merit of white and
    monochromatic light for the determination of visibility by back-
    scattering measurements. Appl. Opt., 4, 501-506.

van de Hulst, H. C., 1957: Light Scattering by Small Particles.
    John Wiley and Sons, 470 pp.

Viezee, W., J. Oblanas and R. T. H. Collis, 1972: Slant range visibil-
    ity measurement for aircraft landing operations. AFCRL-72-0154,
    Air Force Cambridge Research Laboratories, 100 pp. (AD 742359)

_____, _____ and _____, 1973: Evaluation of the lidar technique of
determining slant range visibility for aircraft landings opera-
tion. AFCRL-TR-73-0708, Stanford Research Institute, 136 pp.
(AD 776054)

Vogt, H., 1968:   Visibility measurement using backscattered light.
J. Atmos. Sci., 25, 912-918.

Winstanley, J. V., and M. J. Adams, 1975: Point Visibility Meter:
a forward scatter instrument for the measurement of aerosol
extinction coefficient. Appl. Opt., 14, 2151-2157.

_____, _____ and _____, 1973: Evaluation of the lidar technique of determining slant range visibility for aircraft landings operation. AFCRL-TR-73-0708, Stanford Research Institute, 136 pp. (AD 776054)

Vogt, H., 1968: Visibility measurement using backscattered light. J. Atmos. Sci., 25, 912-918.

Winstanley, J. V., and M. J. Adams, 1975: Point Visibility Meter: a forward scatter instrument for the measurement of aerosol extinction coefficient. Appl. Opt., 14, 2151-2157.